NUREG/CR-0340
ORNL/NUREG/TM-244

LMFBR Aerosol Release and Transport Program Quarterly Progress Report for April–June 1978

T. S. Kress
A. L. Wright

Prepared for the U.S. Nuclear Regulatory Commission
Office of Nuclear Regulatory Research
Under Interagency Agreements DOE 40-551-75 and 40-552-75

OAK RIDGE NATIONAL LABORATORY
OPERATED BY UNION CARBIDE CORPORATION · FOR THE DEPARTMENT OF ENERGY

Printed in the United States of America. Available from
National Technical Information Service
U.S. Department of Commerce
5285 Port Royal Road, Springfield, Virginia 22161

NUREG/CR-0340
ORNL/NUREG/TM-244
Dist. Category R7

Contract No. W-7405-eng-26

Engineering Technology Division

Advanced Reactor Systems Section

LMFBR AEROSOL RELEASE AND TRANSPORT PROGRAM QUARTERLY PROGRESS REPORT FOR APRIL–JUNE 1978

Program Manager: T. S. Kress
Report Coordinator: A. L. Wright

Manuscript Completed — September 29, 1978
Date Published — November 1978

NOTICE: This document contains information of a preliminary nature. It is subject to revision or correction and therefore does not represent a final report.

Prepared for the
U.S. Nuclear Regulatory Commission
Office of Nuclear Regulatory Research
Washington, D.C. 20555
Under Interagency Agreements DOE 40-551-75 and 40-552-75

NRC FIN No. B0121

Prepared by the
OAK RIDGE NATIONAL LABORATORY
Oak Ridge, Tennessee 37830
operated by
UNION CARBIDE CORPORATION
for the
DEPARTMENT OF ENERGY

CONTENTS

FOREWORD

This report summarizes progress under the LMFBR Aerosol Release and Transport Program (sponsored by the Division of Reactor Safety Research of the Nuclear Regulatory Commission) for the period April–June 1978.

Work on this program was initially reported as Volume III of a four-volume series entitled *Quarterly Progress Report on Reactor Safety Programs Sponsored by the NRC Division of Reactor Safety Research.* Prior reports of this series are

Report No.	Period covered
ORNL/TM-4655	April–June 1974
ORNL/TM-4729	July–September 1974
ORNL/TM-4805	October–December 1974
ORNL/TM-4914	January–March 1975
ORNL/TM-5021	April–June 1975

Beginning with the report covering the period July–September 1975, work under this program is now being reported as *LMFBR Aerosol Release and Transport Program Quarterly Progress Report*. Prior reports under this title are

Report No.	Period covered
ORNL/NUREG/TM-8	July–September 1975
ORNL/NUREG/TM-9	October–December 1975
ORNL/NUREG/TM-35	January–March 1976
ORNL/NUREG/TM-59	April–June 1976
ORNL/NUREG/TM-75	July–September 1976
ORNL/NUREG/TM-90	October–December 1976
ORNL/NUREG/TM-113	January–March 1977
ORNL/NUREG/TM-142	April–June 1977
ORNL/NUREG/TM-173	July–September 1977
ORNL/NUREG/TM-193	October–December 1977
ORNL/NUREG/TM-213	January–March 1978

Copies of all these reports are available from the Technical Information Center, Oak Ridge, Tennessee 37830.

SUMMARY

A. L. Wright

The Aerosol Release and Transport (ART) Program at ORNL is designed to investigate the relase and transport of radionuclides that may result from a hypothetical core-disruptive accident (HCDA) in a liquid-metal-cooled fast breeder reactor (LMFBR). The experimental program is being conducted in three facilities: the CRI-II, NSPP, and FAST/CRI-III. The analytical effort is designed to support the experiments as well as to provide independent assessments of the consequences of an HCDA.

During this reporting period, testing continued in the FAST/CRI-III facility. Eight tests were performed in the CRI-III vessel and one in the FAST vessel. These consisted of seven tests of the FAST under-sodium sample design, one low-pressure test in preparation for the planned "Sandia normalization" tests, and one exploratory test in which the capacitor banks were fired sequentially (three initially and three 10 msec later).

Two of the FAST vaporizer tests used the short (8.8-cm-long) sample that had been used successfully in previous experiments; the other five tests employed the long (∿10.8-cm) sample used in CRI-III energy density tests. While four of the tests with the long stack were unsuccessful, the last test (done in the FAST vessel) was successful, indicating that the test problems may have been solved.

In the low-pressure test, arcing occurred at ∿1 msec, but the quartz tube was not broken; however, this is an improvement over the low-pressure test done last quarter.

The sequential bank firing was quite successful; a large energy input resulted in a large amount of aerosol being produced.

The first shakedown test was performed in the FAST vessel this quarter. The PDP/8A data acquisition system for FAST water and sodium tests was installed and made operational.

The third test of the U_3O_8 consumable electrode aerosol generator for the NSPP was performed this quarter. Data on aerosol concentration and aerodynamic size vs time are presented and compared with data collected in the two previous U_3O_8 tests. As in the two previous tests, the aerosol concentration was low.

The first NSPP mixed-oxide aerosol experiment was performed at the end of the reporting period. The uranium oxide aerosol was produced first using the consumable electrode aerosol generator; after allowing this aerosol to mix in the vessel, sodium oxide aerosol was produced by a sodium pool fire. The target sodium-to-uranium oxide mass ratio was 10:1. Results will be reported next quarter.

Experiments were performed in CRI-II in an effort to develop a high-capacity U_3O_8 aerosol generator for use in the NSPP experiments. Aluminum oxide aerosols were produced using the plasma torch technique. A version of the plasma torch is now being set up for use in the NSPP. Use of this torch as an aerosol generator will hopefully allow the production of high concentrations of uranium oxide aerosol.

Samples of uranium oxide aerosols collected in CRI-II were analyzed chemically and by x-ray diffraction for identification of the oxygen-to-uranium ratio and the crystal form of the oxide. This method will be used routinely to confirm the form of the oxide aerosol produced by the metal-oxygen torch.

In the analytical program, a CSMP computer code was generated to model a FAST experiment and the rise of a UO_2 bubble in a CDA. Condensation heat transfer at the bubble interface is modeled using the Özisik-Kress analysis performed previously; in addition, radiation heat transfer and interface heating by beta-emission from fission products are included. Calculations presented are for parametric values of condensation heat transfer coefficient, bubble diameter, and internal heat generation rate.

The AEROSIM computer program, a British code developed to calculate aerosol transients, and the associated differential equation solver FACSIMILE were made operational. Comparisons with HAARM-2 and HAARM-3 calculations were made but not reported.

GLOSSARY OF ACRONYMS

ACPR	Annular Core Pulsed Reactor
AF	Arc Furnace
ART	Aerosol Release and Transport
CDA	Core-Disruptive Accident
CDV	Capacitor Discharge Vaporization
CRI	Containment Research Installation
CSMP	Continuous System Modeling Program
FAST	Fuel Aerosol Simulant Test Facility
HCDA	Hypothetical Core-Disruptive Accident
LMFBR	Liquid-Metal Fast Breeder Reactor
NRC	Nuclear Regulatory Commission
NSPP	Nuclear Safety Pilot Plant
ORNL	Oak Ridge National Laboratory
PT	Plasma Torch

LMFBR AEROSOL RELEASE AND TRANSPORT PROGRAM QUARTERLY PROGRESS REPORT FOR APRIL—JUNE 1978

T. S. Kress

ABSTRACT

This report summarizes progress for the LMFBR Aerosol Release and Transport Program, sponsored by the Division of Reactor Safety Research of the Nuclear Regulatory Commission, for the period April—June 1978. The program is designed to investigate radionuclide release and transport from LMFBRs for reactor events of severity up to and including hypothetical core-disruptive accidents. Topics discussed include recent capacitor discharge vaporization tests in the CRI-III facility and the first shakedown test the the FAST facility; FAST facility installation progress; performance tests for the consumable electrode aerosol generator for the NSPP and comparison of results from three performance tests; performance of the first mixed sodium oxide and uranium oxide test in the NSPP; development of the backup plasma torch aerosol generator for use in generating high uranium oxide aerosol densities in the NSPP; and progress in development of a computer model to calculate the behavior of UO_2 vapor bubbles produced in core-disruptive accidents and in fuel-aerosol simulant test facility experiments.

Keywords: aerosol, hypothetical accident, breeder reactor, fission product release, fission product transport, ex-reactor experiment, safety, radionuclide transfer, plutonium.

1. INTRODUCTION

The LMFBR Aerosol Release and Transport (ART) Program at ORNL, sponsored by the Division of Reactor Safety Research of the Nuclear Regulatory Commission (NRC), is an LMFBR safety program concerned with radionuclide release and transport. The scope includes radionuclide release from fuel, transport to and release from primary containment boundaries, and behavior within containments. The overall goal of the program is to provide the analytical methods and experimental data necessary to assess the quantity and transient behavior of radionuclides released from LMFBR cores as a result of postulated events of varying severity up to and including severe hypothetical core-disruptive accidents (HCDAs).

The program is divided into several related experimental and analytical activities as summarized below:

1. development of a capacitor discharge vaporization (CDV) system for deposition of energy in simulated LMFBR fuel (UO_2) which will provide a nonnuclear means for studying the fuel response to HCDA-like energy depositions;
2. development of alternative means for generating fuel-simulant aerosols on a relatively continuous basis;
3. study of the characteristics and behavior of fuel-simulant aerosols in several small vessels, including the effects of radiation and the simultaneous vaporization of small amounts of sodium;
4. production and study of fuel-simulant and sodium aerosols in the Nuclear Safety Pilot Plant (NSPP) for validation of models with particular emphasis on scaling features relative to containment size;
5. study of the fuel interactions, expansion, and thermal behavior within the sodium pool as the resultant fuel vapor bubble is transported through the sodium to the cover-gas region.

Varying levels of effort are anticipated within these categories, with analytical modeling accompanying the experimental work. The analytical requirements fall into four categories: (1) predisassembly analyses using existing models to establish conditions at the start of disassembly, (2) fuel response to high rates of energy deposition, (3) fuel-bubble dynamic behavior and transport characteristics under sodium, and (4) dynamic aerosol behavior at high concentrations in the bubble and containment atmospheres.

An attempt will be made to consolidate the analyses and data and to present them in a manner which will facilitate direct assessment of the radiological hazard associated with arbitrary hypothetical accident scenarios.

2. EXPERIMENTAL PROGRAM

2.1 CRI-III and FAST Experiments

A. L. Wright J. M. Rochelle
A. M. Smith J. S. White

2.1.1 Introduction

Nine tests were performed in the combined FAST/CRI-III facility: eight in the CRI-III and one in the FAST vessel. These tests were of three types:

1. seven FAST vaporizer design tests, two (CDV 44 and 46) using the short sample ($\sim$8.8-cm length) successfully tested last quarter[1] and five (CDV 47 through 50 and FAST 1) using the long ($\sim$10.8-cm) samples typical of previous CRI-III energy density tests;
2. an exploratory test (CDV 45) in which the capacitor banks were fired sequentially (i.e., three initially and three 10 msec later);
3. one test at low vessel pressure (approximately 150 μ) in support of the "Sandia normalization" tests to be performed later in CRI-III (CDV 43).

Data for these tests are presented in Table 1 to 3. Individual test results and conclusions are presented in the following three sections.

Table 1. Sample data

Test	Pellet stack mass (g)	Pellet stack length (cm)	Microsphere mass (g)	Quartz tube dimensions (cm)	
				ID	OD
CDV 43	22.63	10.87	38.24	1.02	1.70
CDV 44	18.32	8.87	35.16	1.00	1.72
CDV 45	22.47	10.86	33.56	0.97	1.68
CDV 46	18.36	8.86	32.54	1.01	1.72
CDV 47	22.60	10.80	34.27	1.00	1.69
CDV 48	22.69	10.95	37.46	0.99[a]	1.68
CDV 49	21.99	10.64	34.79	0.98	1.69
CDV 50	22.53	10.80	32.40	0.95[b]	1.68
FAST 1	22.72	11.02	33.49	0.95	1.67

[a] Average; low-voltage end = 0.98 cm, high-voltage end = 1.00 cm.
[b] Average; low-voltage end = 0.96 cm, high-voltage end = 0.95 cm.

Table 2. High preheat, CDV charging data

Test	High preheat power (W)	Sample resistance after preheat (Ω)	High preheat time (sec)	Time between preheats (sec)	Number of capicitor banks charged	Charge voltage (V)	Initial bank energy (kJ)
CDV 43	2200	[a]	28	2	6	1450	62
CDV 44	1700	0.5	28	2	3	2250	75
CDV 45	2200	0.52	28	2	6[b]	1450	62
CDV 46	1700	0.5	28	2	2	2500	60
CDV 47	2100	0.5	28	2	4	1950	75
CDV 48	2100	0.68	28	2	4	1950	75
CDV 49	1900	0.58	28	2	4	1950	75
CDV 50	2000	0.65	28	2	4	1950	75
FAST 1	2000	0.52	28	2	4	2143	91

[a]Resistance could not be measured.

[b]Sequential firing: three initially and three 10 msec later.

Table 3. Energy input, aerosol yield data

Test	CDV time to arcing (msec)	CDV energy deposition before arc (kJ)	Estimated initial aerosol yield (g/m^3)	Estimated initial aerosol mass[a] (g)
CDV 43	1.16	5.73	0	0
CDV 44	2.32	34.0	3.53	1.98
CDV 45	10.9	36.2	9.93	5.56
CDV 46	1.17	20.4	0.26	0.15
CDV 47	2.65	27.7	0.86	0.48
CDV 48	0.66	4.4	1.08	0.61
CDV 49	3.25	30.6	0.54	0.30
CDV 50	>18[b]	61.6	0.42	0.24
FAST 1	2.26	30.7	[c]	[c]

[a]Based on vessel volume = 0.56 m^3.

[b]No arc produced for time <18 msec; 61.6 kJ deposited to sample up to that time.

[c]No aerosol mass measurements made.

2.1.2 FAST vaporizer design test results

Seven tests were performed this quarter to evaluate the vaporizer design to be used in the under-sodium experiments. Two tests used the ∿8.8-cm pellet stack length employed in previous successful FAST design tests (CDV 39 through 42), and the other five used an ∿10.8-cm pellet stack, the length of that used in CRI-III energy density test samples. This longer length is preferable in order to allow comparisons of FAST vaporizer test results with those of previous energy density tests.

Test CDV 44. Conditions for this test were similar to those for CDV 42, except that the electrode-quartz clearance was 0.018 cm (0.007 in.) rather than the 0.033-cm (0.013-in.) clearance in CDV 42. This smaller clearance should decrease end material leakage during CDV and thus result in rapid UO_2 pressurization and early sample breakup. Sample rupture occurred at 2.32 msec, about 1 msec earlier than in CDV 42. Posttest sample examination showed that less UO_2 had been pushed back into the high-voltage end of the test assembly. These results are a good indication that the reduced clearance had the desired effect. The 1.98-g yield was about half that produced in CDV 42; however, the CDV energy input for test 42 was also about 15 kJ greater.

Test CDV 46. In previous FAST vaporizer tests, three, four, or five capacitor banks were used for the discharge phase. In this test, two banks were used to observe the effect of increased energy discharge rate to the test sample on breakup time and aerosol yield. An arc was produced early after capacitor discharge (1.17 msec). Although a substantial amount of energy (20.4 kJ) was input, steel tube rupture was incomplete and little aerosol was produced.

Posttest examination of the test assembly showed that the arc occurred in the steel housing in the region where the nickel conducting rod and high-voltage electrode are joined. Indications were that a lavite insulator broke (for unknown reasons) prematurely, allowing the arc to occur. This arc stopped the energy input to the test sample before sufficient internal pressure was built up to rupture the quartz and steel tubes.

Test CDV 47. This was the first FAST vaporizer test with the $\sim$10.8-cm sample length used previously in CRI-III energy density tests. Increasing the pellet length necessitated a higher preheat (2100 W) to produce a sample resistance of roughly 0.5 Ω.

CDV energy input was good (27.7 kJ), but steel tube rupture was poor and little aerosol was formed. Examination of the sample after the test showed that most of the quartz tube remained in large pieces; this was not typical of sample breakup produced by UO_2 internal pressurization. The early cutoff of CDV energy input could have been due to (1) quartz rupture during preheat, which could have resulted from the 2000 W preheat coupled with the quartz-electrode clearance of 0.013 cm (0.005 in.), the smallest used to date; or (2) an arc in the high-voltage end of the test assembly (however, no definite evidence of this was found).

Test CDV 48. This was the second attempt to perform a FAST vaporizer test with a sample having the CRI-III pellet stack length. During the 500-W low preheat, a hot spot near the low-voltage end of the test sample caused a small hole to melt in the steel tube. The test continued, but high preheat and CDV were erratic. Arcing occurred in less than 1 msec, and little aerosol was formed.

Posttest examination of the sample showed that there had been a direct electrical path from the pellets to the portion of the steel tube where the hole was formed. It is probable that quartz rupture during low preheat produced this current path. Previous FAST vaporizer test samples were loaded with ~0.32 cm (0.125 in.) of microsphere packing extended over the pellets at the low-voltage end of the sample. This compensated for settling of microspheres after loading and was thought to cushion the pellets to prevent them from cracking when the sample was assembled. In CRI-III tests with similar microsphere loading at the high-voltage end, arcing had always been observed in this initial stage of sample preheat; such arcing could have caused a hot spot and quartz rupture in CDV 48. In subsequent FAST vaporizer tests, the excess microsphere packing will be reduced and the initial sample preheat will be slower to try to minimize the amount of arcing.

Test CDV 49. The major difference between this test and CDV 47 and 48 was that the preheat level was lowered to guard against premature steel tube melting. The CDV 49 preheat was quite stable, and the 0.58-Ω sample resistance was only slightly greater than the 0.5 Ω previously achieved. However, although CDV energy deposition time (3.25 msec) and input (30.6 kJ) were good, steel tube rupture and aerosol production were poor.

Posttest examination of the sample assembly showed that arcing had occurred at the high-voltage end and had probably cut off CDV energy input and prevented efficient quartz (and steel) tube breakup. Such arcing may also have caused the poor results produced in CDV 47. The arc was probably caused by material leakage from the high-voltage end of the test sample. In later tests, the high-voltage electrode length will be 5.72 cm (2.55 in.) in an effort to eliminate the arc path. This increased electrode length [the old length was 3.18 cm (1.25 in.)] will result in less material leakage and also produce a longer path between the electrode and other conducting surfaces (a lavite insulator separates the electrode and the test assembly housing).

Test CDV 50. The major change in this test was that a 5.72-cm-long (2.25-in.) high-voltage electrode was used [2.54 cm (1 in.) longer than that used previously] in an effort to eliminate premature arcing in the test assembly. During the 500-W low preheat, sample resistance was 14 Ω, roughly twice the normal value. Because of this, the resistance after high preheat was also larger than the normal 0.5 Ω. No arcing occurred, indicating that a majority of the 75-kJ initial charge went into the sample; however, steel rupture and aerosol production were poor.

The quartz tube did not rupture during the test and little UO_2 remained inside it. Lengthening the high-voltage electrode had the desired effect of preventing material leakage out of the high-voltage end; however, almost all of the material in the tube went out of the low-voltage end (the first time this had occurred to a significant degree). In retrospect, the quartz-electrode clearance of 0.033 cm (0.013 in.) on the low-voltage end may have been too large. However, this was the most successful FAST vaporizer test to date using the ~10.8-cm-long samples because the arcing problem appeared to have been eliminated. Reduced quartz-electrode clearance at the low-voltage end of the sample should allow subsequent tests to be performed successfully.

Test FAST 1. This test, the first shakedown test performed in the FAST vessel, used the FAST vaporizer design with the long pellet stack. The quartz-electrode clearance was held to about 0.020 cm (0.008 in.) on the high- and low-voltage ends, and the high-voltage electrode was again 5.72 cm long (2.25 in.). Since no mass sampling instrumentation was ready for installation, this test was a check of all electrical connections to FAST and an attempt to successfully test the vaporizer unit.

The steel tube was successfully broken and a significant amount of aerosol was observed visually. Figure 1 shows the test unit after capacitor discharge inside the vessel.

It is interesting to compare the energy input for FAST 1 with that of CDV 47 and 49. All three tests had comparable energy inputs; however, only FAST 1 was a success. This success is attributed to elimination of the arcing and material leakage problems, thus allowing sufficient UO_2 pressure to build up to burst the quartz and stainless tubes.

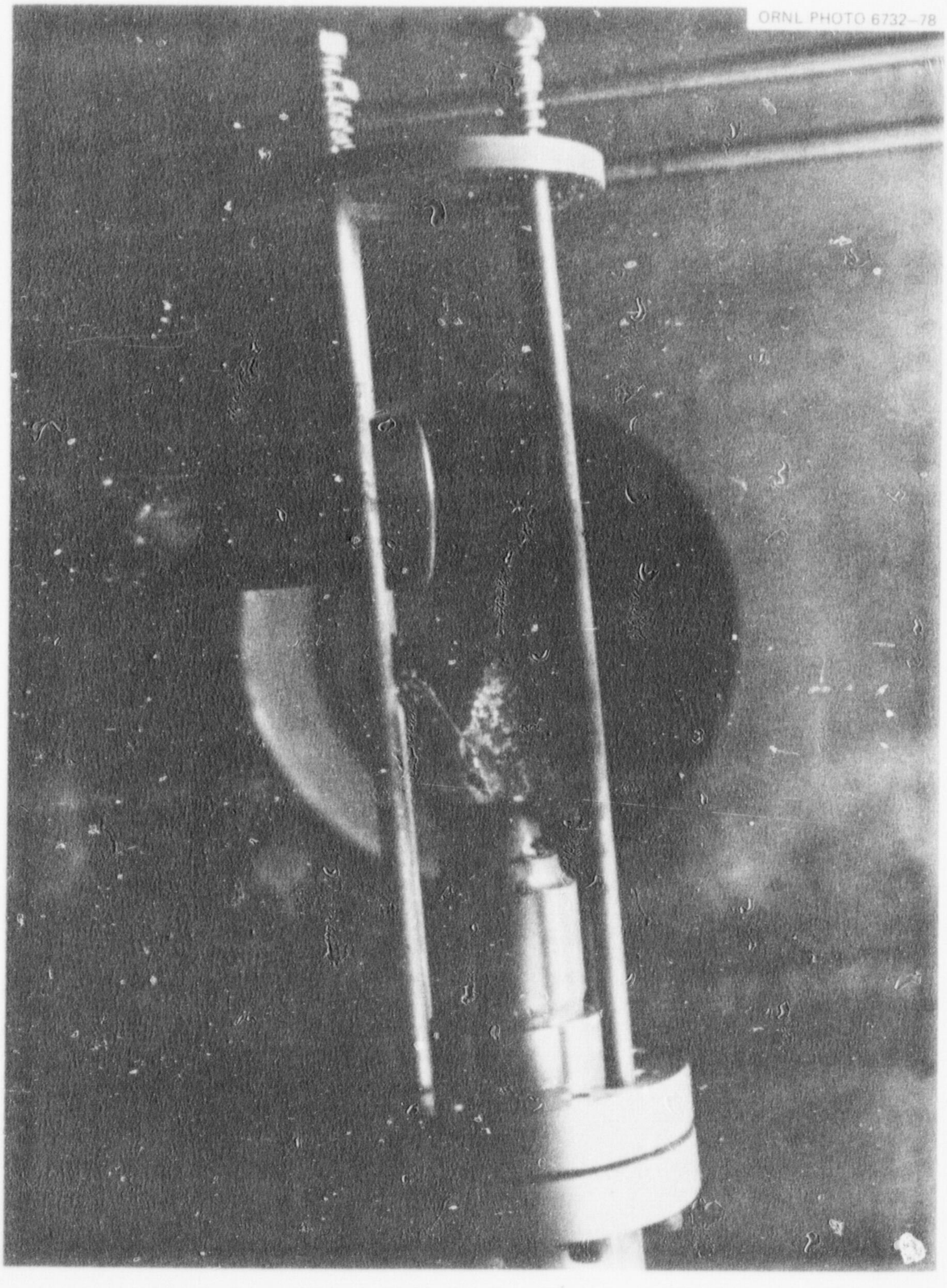

Fig. 1. FAST vaporizer after CDV, seen through sight port of the FAST vessel.

Summary. Several problems were encountered in trying to perform FAST vaporizer tests with the longer pellet stack, but they appear to have been solved. After a few more successful tests of the FAST vaporizer in CRI-III, we will be able to begin the first phase of testing in the FAST vessel (vaporizations in argon). In addition, FAST vaporizer tests in water in the CRI-III vessel will start early next quarter.

2.1.3 Sequential bank firing test in CRI-III

The inability to choose the amount of, and time for, energy input has been one of the drawbacks in conducting tests efficiently using the CDV technique. Test CDV 45 was an attempt to control the energy input by firing the capacitor banks in sequence, three initially and three 10 msec later. The firing of the first three banks is analogous to an additional preheat; thus when the other three are fired, the energy input rate should be drastically increased due to lowered sample electrical resistance.

This very interesting and successful test proceeded exactly as planned. Figure 2 shows the voltage and current traces. The second discharge occurred at 9.68 msec, with 25.8 kJ input up to that time, and sample breakup occurred at 10.9 msec. After high preheat, the sample resistance was 0.55 Ω, but at 9.68 msec this had been reduced to 0.20 Ω. As expected, the rate of energy input during the second discharge was large, more than twice that during the first discharge. In addition, the aerosol yield of 5.56 g was the second best achieved to date in a CRI-III experiment.

The results from this technique indicate that more tests should be performed at various charging levels and times for the final discharge to see if the energy input and input time can really be controlled.

2.1.4 Low-pressure test performed in support of "Sandia normalization" experiments

As discussed in the previous quarterly,[1] a series of tests in the CRI-III vessel at low pressure will be performed. The expanding fuel material produced by CDV will be sampled with a spinning wheel collector developed at Sandia to determine drop sizes and velocities. This will

ORNL PHOTO 4631–78

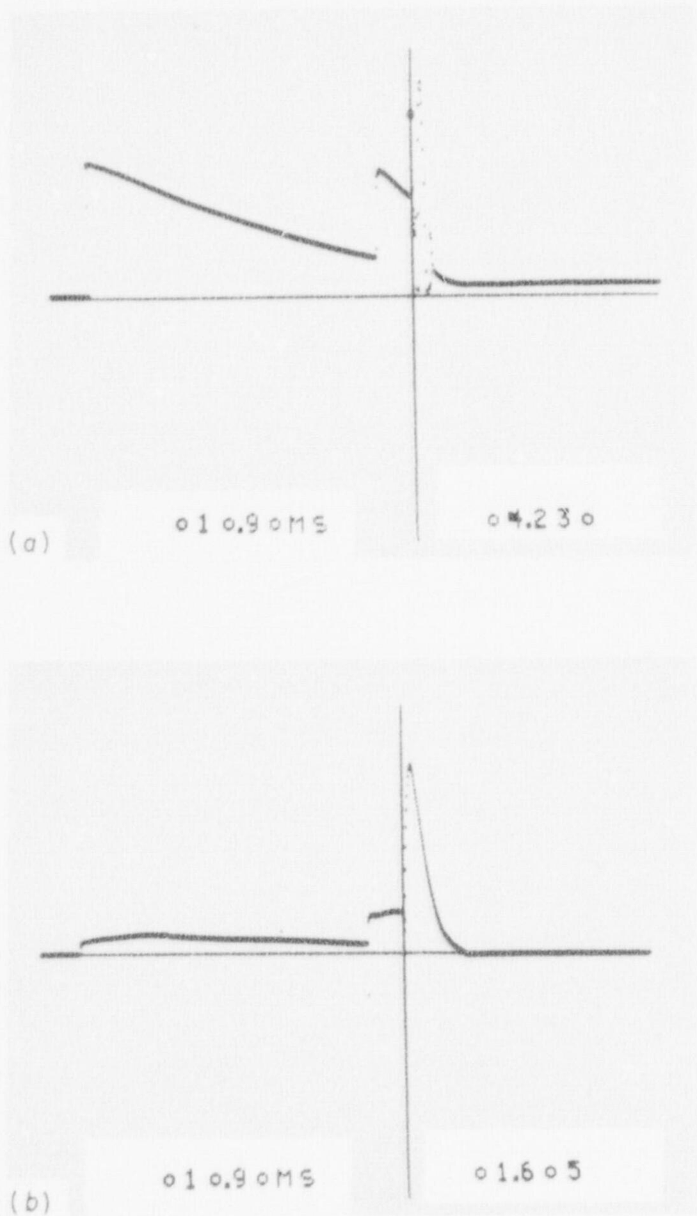

Fig. 2. Capacitor discharge voltage vs time for CDV 45 (*a*); capacitor discharge current vs time for CDV 45 (*b*).

allow us to compare drop sizes and velocities produced by electrical (CDV) and neutronic breakup [in Sandia'a Annular Core Pulsed Reactor (ACPR)] at comparable energy levels.

In the previous attempt to conduct a low-pressure test, arcing occurred between the copper conducting electrode and the steel housing of the CRI-III vaporizer. For CDV 43, insulators were put over the electrode to attempt to eliminate this arc path. The vessel pressure was 150 μ when preheat was started; there was observable arcing at the high-voltage end of the assembly, but we were able to proceed with sample preheat. In this test (as opposed to CDV 35), a small amount of energy was input to the sample during CDV. However, the tube did not break at arcing and no aerosol was formed. Posttest examination of the sample showed that arcing and melting had occurred at the junction between the copper rod and high-voltage electrode; the high-speed movies indicated that the arc may have been produced by material leakage out of the tube. In the next vacuum test, the length of the high-voltage electrode will be increased in an effort to eliminate the arcing problem.

2.1.5 Preparation of FAST facility for testing

As discussed in the previous section, the first shakedown test in the FAST facility (Fig. 3) was performed this quarter. This test proved that all electrical systems needed to operate the CDV system in the FAST facility were properly made.

In this shakedown test, we attempted to heat the FAST vessel, up to the 866 K (1100°F) maximum operating temperature for the sodium tests. We were not able to achieve this temperature because of excessive heat losses from the vessel head. Additional thermal insulation should solve this problem.

The FAST data acquisition system was installed and checked out this quarter. Figure 4 shows the equipment in the FAST/CRI-III control room. This system is primarily for use in the FAST water and sodium tests. Instrumentation leads to the data system were extended into the control room and are ready to be connected.

2.2 Secondary Containment Aerosol Studies in the NSPP

R. E. Adams L. F. Parsly

2.2.1 Introduction

Activities at the NSPP during this period included the performance of uranium oxide aerosol experiment 203, analysis of the data from the

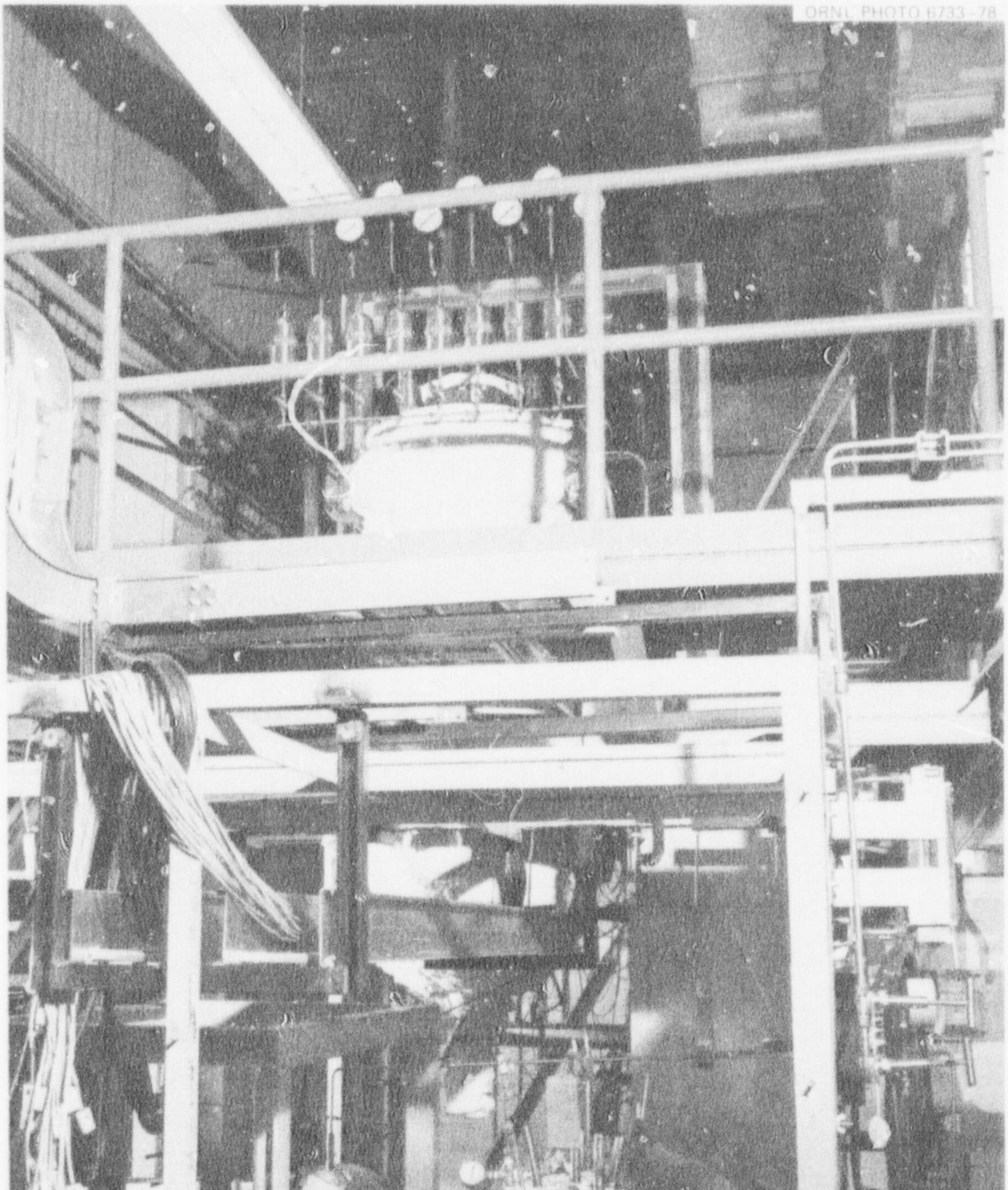

Fig. 3. FAST vessel.

ORNL PHOTO 6734-78

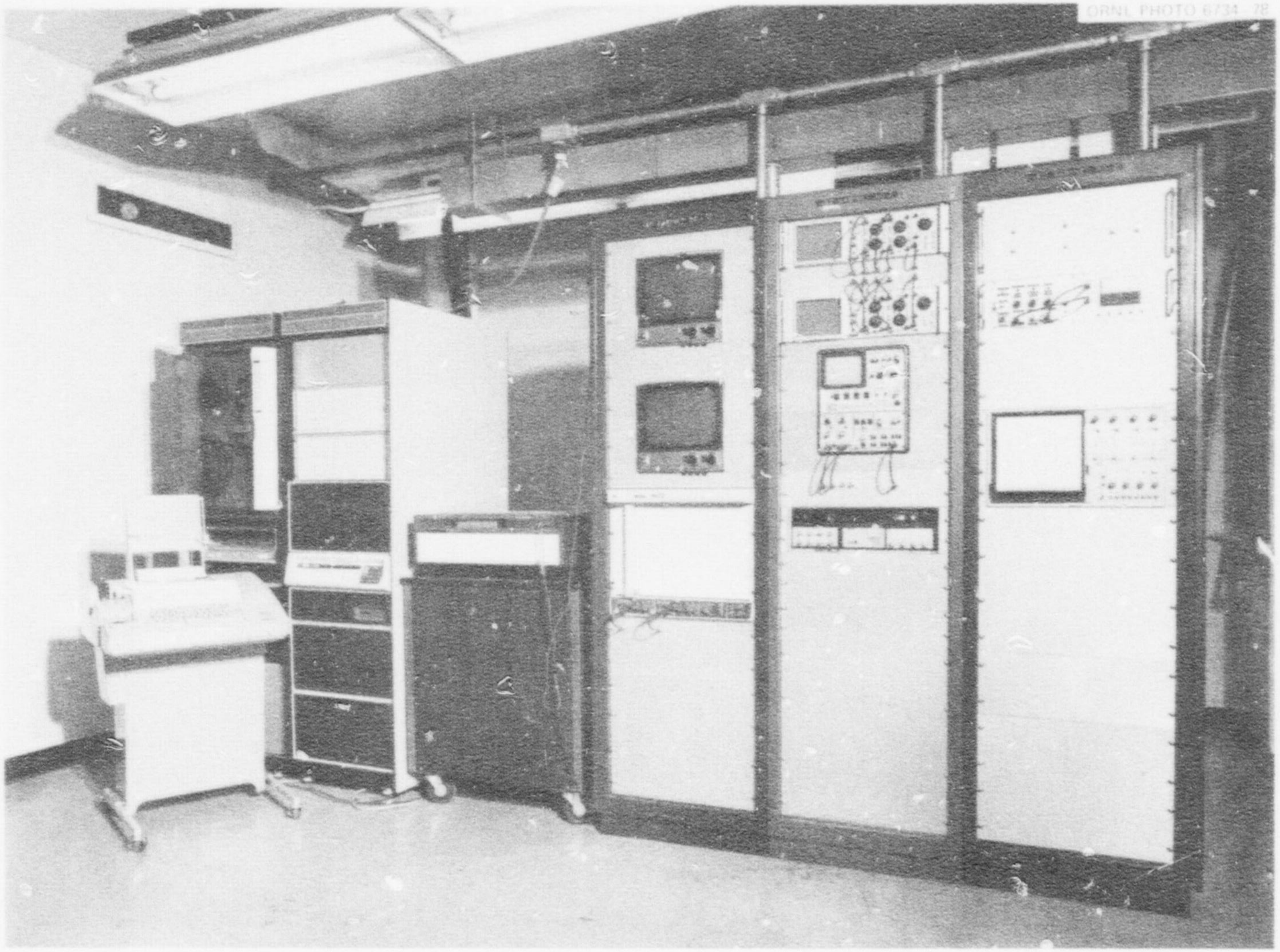

Fig. 4. FAST/CRI-III control room, showing PDP/8A data acquisition system on the left and data acquisition equipment for preheat and capacitor discharge on the ight.

experiment, and preparation for and performance of the first mixed uranium oxide and sodium oxide aerosol experiment 301.

2.2.2 Uranium oxide aerosol experiment 203

Uranium oxide aerosol experiment 203 was the third and last of the planned series to establish the performance characteristics of the consumable electrode aerosol generator. Test procedures and operation of the aerosol generator have been reported previously.[1] This experiment differed slightly from experiments 201 and 202 in that the dc arc power and the argon shield gas flow rate were decreased in an effort to achieve a larger aerosol concentration within the test vessel. An increase in aerosol concentration was noted, but the level was still below the desired range.

The vessel initially contained relatively dry air (initial relative humidity was about 10%), and the temperature and pressure were ambient. A small resistance heater rod in the bottom of the vessel maintained convective currents within the vessel atmosphere to provide for mixing of the aerosol. Approximately 15 cm (6 in.) of the 2.54-cm-diam (1.0-in.) uranium metal electrode was removed by the arc over the 18.5-min duration of aerosol generation. As before, the major portion of this material fell into the catch pan below the electrode holder as a granular black residue of U_3O_8. Aerosol parameters measured were airborne mass concentration, particle size, and fallout and plateout rates.

Aerosol and mass concentration. Aerosol mass concentrations were measured with two types of filter samplers. The in-vessel samplers are self-contained units mounted internally and controlled remotely. The wall aerosol samplers penetrate the vessel wall through a ball valve and are constructed so that filter packs may be inserted and removed manually during the experiment.

Results obtained from both types of filter samplers are shown in Fig. 5. A maximum aerosol concentration of about 0.2 g/m^3 (1.25×10^{-5} lb/ft^3) was indicated about 60 min after start of aerosol generation; the concentration decreased to about 0.0015 g/m^3 (9.35×10^{-8} lb/ft^3) at the termination of the experiment (48 hr).

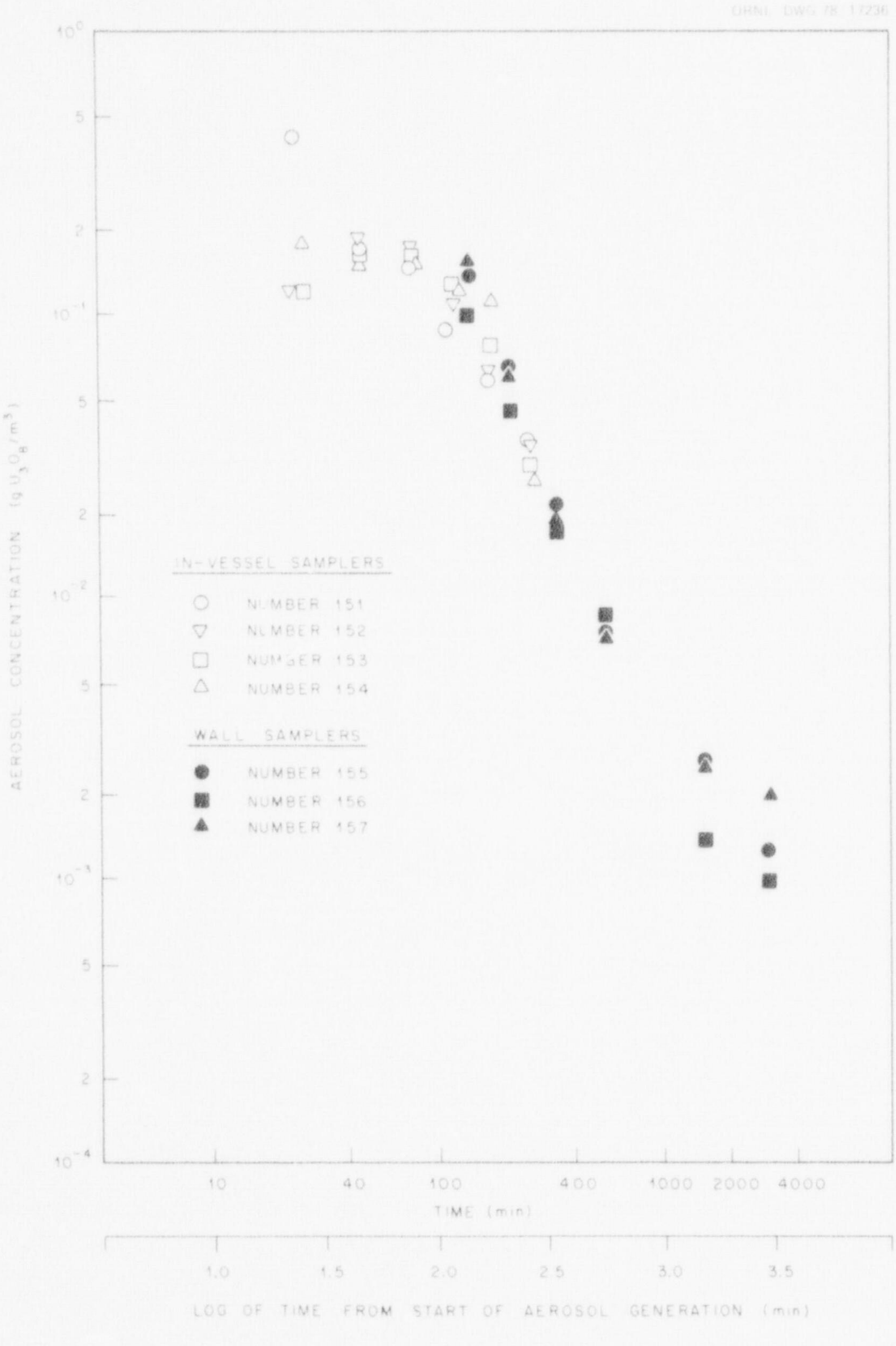

Fig. 5. Uranium oxide aerosol mass concentration for experiment 203.

Aerosol particle size. The sizes of the agglomerated particulates were measured over the first 24 hr of the experiment. Seven aerosol samples were taken with an eight-stage cascade impactor (Andersen Mark III). Results from these measurements are given in Table 4.

Table 4. Uranium oxide aerosol particle size — experiment 203

Sample	Time after start of aerosol generation (min)	Equivalent aerodynamic diameter, d_{50} (μ)	Geometric standard deviation (σ_g)
1	28	1.0	2.0
2	54	1.7	2.1
3	118	3.2	2.4
4	221	2.8	2.7
5	335	1.7	2.5
6	585	1.5	2.5
7	1487	0.8	2.8

Distribution of aerosol. At the termination of the experiment (48 hr), the approximate distribution of aerosol as determined by the total fallout and plateout coupons and final filter samples was as follows: aerosol settled onto floor, 81.6%; aerosol plated onto interior surfaces, 17.7%; and aerosol still suspended in the vessel atmosphere, 0.7%.

2.2.3 Comparison of data from uranium oxide aerosol experiments

Aerosol mass concentration. Figure 6 illustrates the behavior of aerosol mass concentration as a function of time for experiments 201, 202, and 203. Values plotted are average for all filter samples taken at each time point. These data indicate that the removal rate of aerosol from the vessel atmosphere increases as the initial mass concentration of the aerosol increases.

Aerosol particle size. Figure 7 compares the aerosol particle size as measured by cascade impactors for the three uranium oxide experiments.

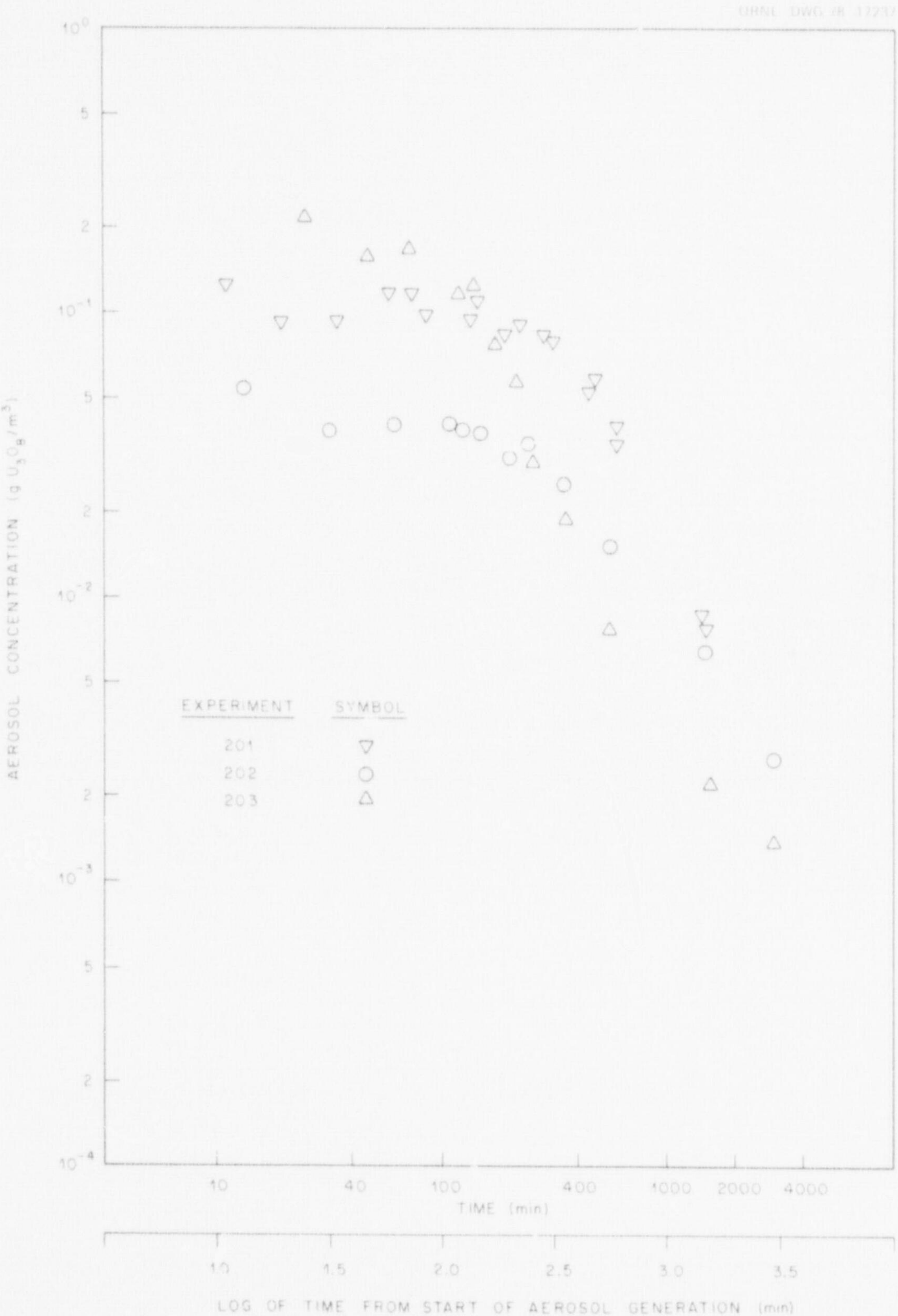

Fig. 6. Uranium oxide aerosol mass concentration for experiments 201, 202, 203.

ORNL DWG 78 17238

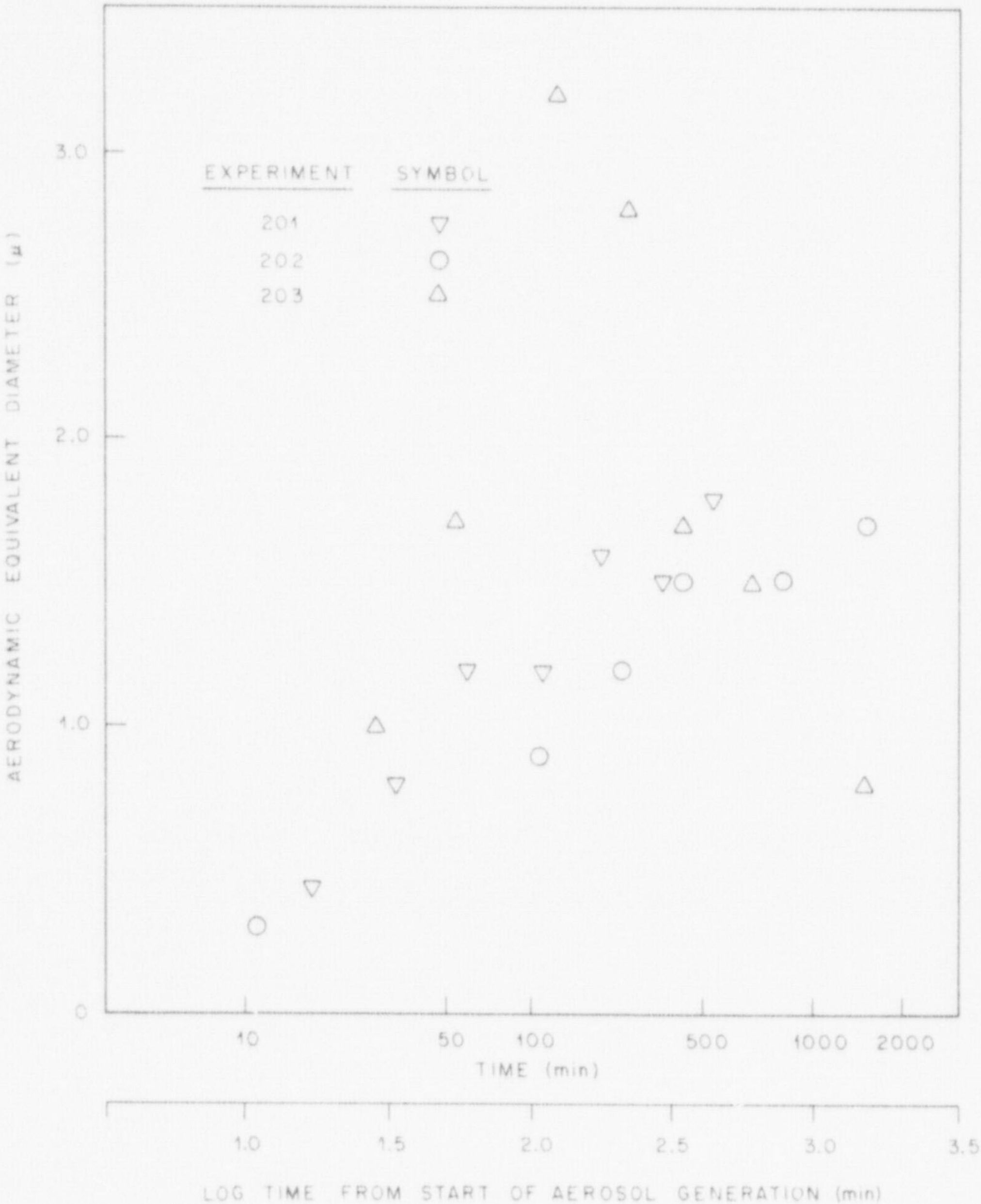

Fig. 7. Uranium oxide aerosol particle size for experiments 201, 202, 203.

The aerosol produced in experiments 201 and 202 increased in size (equivalent aerodynamic diameter) over the duration of the experiment, with the maximum size indicated at the end of the period of measurement. The behavior in experiment 203 was different; a maximum size was indicated early during the period of measurement and then decreased over the remainder of the experiment.

Distribution of aerosol. Table 5 compares final aerosol distribution for the three experiments. Distributions in experiments 201 and 202 are very similar even though the initial maximum aerosol concentration and the duration of the experiments were different. The similar growth in particle size suggests similar aerosol behavior. Experiment 203 produced a dissimilar aerosol distribution, and the larger indicated growth in particle size could account for the enhanced aerosol fallout and the reduced fraction still suspended in the atmosphere at the termination of the experiment.

Table 5. Final aerosol distributions for uranium oxide test series

	Experiment 201	Experiment 202	Experiment 203
Duration of experiment (hr)	24	48	48
Maximum aerosol concentration achieved (g/m^3)	0.12	0.04	0.20
Aerosol settled onto floor (%)	54	51	81.6
Aerosol plated onto interior surfaces (%)	39	43	17.7
Aerosol still suspended in vessel atmosphere (%)	7	6	0.7

2.2.4 Mixed-oxide aerosol experiment 301

The first experiment in the mixed-oxide aerosol experiment series was conducted at the end of this reporting period. The uranium oxide aerosol was produced with the consumable electrode aerosol generator, using forced air flow around the uranium metal electrode in a further effort to increase aerosol production. After allowing time for the uranium oxide aerosol to mix within the vessel atmosphere, sodium oxide aerosol was produced by a sodium pool fire of about 1 kg (2.2 lb) of sodium. Behavior of the mixed-oxide aerosol was then monitored until the termination of the experiment at 48 hr. The target mass ratio of sodium oxide to uranium oxide was 10:1. Analytical data will not be available until the next reporting period.

2.3 Basic Aerosol Experiments in CRI-II

G. W. Parker   A. L. Sutton, Jr.

2.3.1 Development and testing of the plasma metal-oxygen torch for the NSPP

Following the initial operation of the plasma metal-oxygen torch in CRI-II, as discussed later in this report, a slightly modified version of the torch head was fabricated and is being set up for testing with the Metco plasma gun for the NSPP. The multiple capillary feeder design continues to be reliable in the CRI-II model and therefore has been incorporated in the NSPP model. The present model, the front and back of which are shown in Fig. 8, uses only eight capillary tubes in

ORNL DWG 78-13811

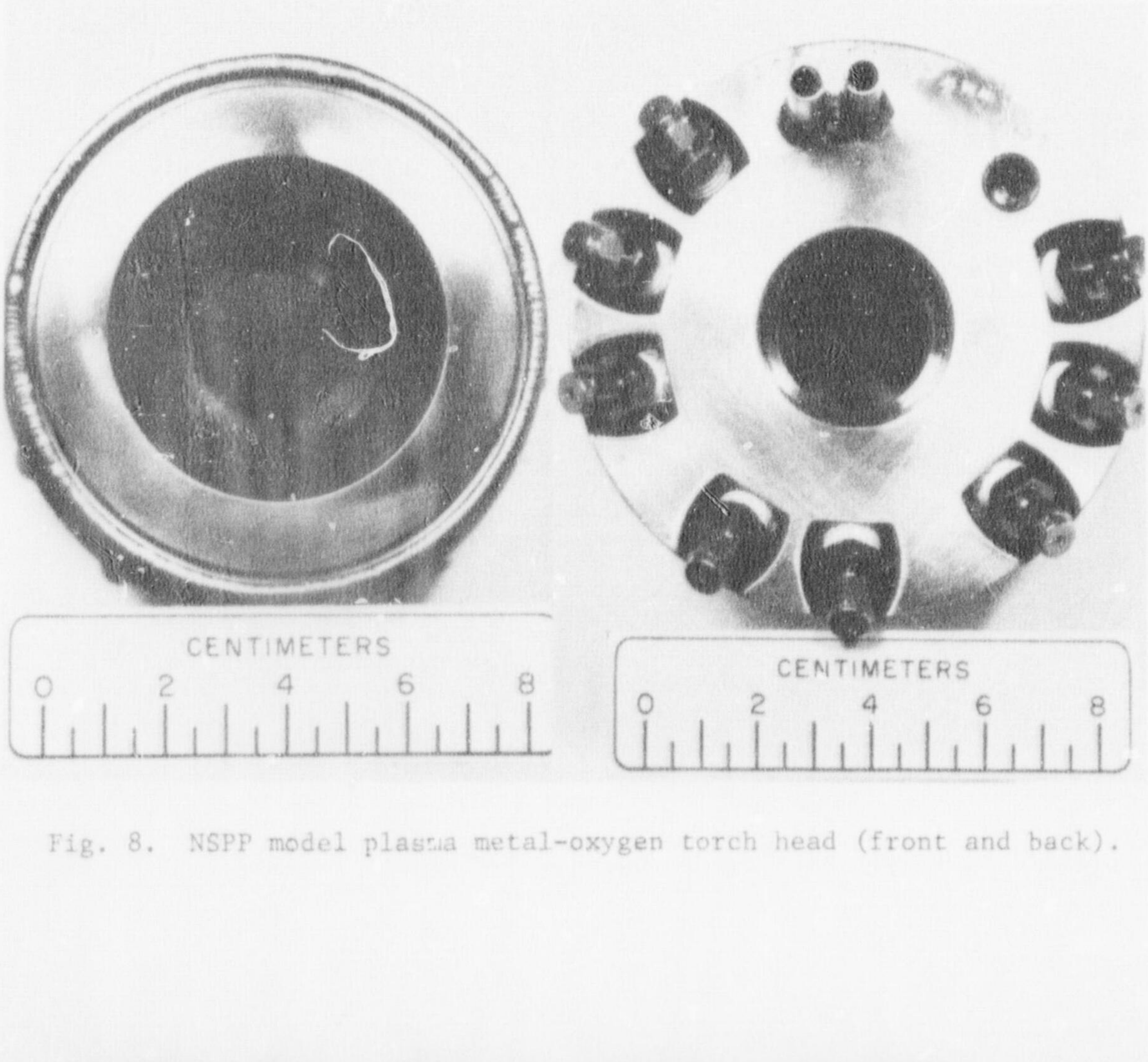

Fig. 8. NSPP model plasma metal-oxygen torch head (front and back).

a single circular pattern since this is the largest diameter head that can be tested in CRI-II. A practical extension of this design, using multiple concentric arrays of up to 30 capillaries, could be developed later if desired. The complete assembly, including all parts for pretesting in CRI-II, is shown in Fig. 9.

2.3.2 Initial aluminum oxide aerosol torch tests in CRI-II

Since our vacuum dry box still requires some upgrading before the powdered uranium can be charged into the feeder, we have continued testing the torch at increasing increments of operating time from 0.5 to 2.0 min to establish control of the flame and reliability of the cooling and feeding mechanism. For the most part, these tests have all been successful, although cooling water has leaked through stress-induced cracks in the torch liner (originally a commercial nickel crucible). We have since refabricated the present liners with stainless steel components.

Control of the torch has been aided by visual monitoring of the flame through two glass-sealed ports (Fig. 10) and by means of recorded temperature and pressure changes in the vessel. For the 2-min burn of aluminum at about 35 g/min, the temperature rise was about 35°C and the pressure change about 5 psi. The maximum aerosol (Al_2O_3 delta-phase) concentration was about 8 g/m^3 (Fig. 11), or about 36 g out of a possible 100. This is about half the yield that we had experienced earlier; however, it is expected that this can be significantly improved.

Of interest is the similarity in size (both Stokes and impactor diameters) (Fig. 12) of the aluminum oxide and uranium oxide aerosols. A plot of the fraction remaining airborne in relation to settling time (Fig. 13) shows only a slightly different attenuation rate without differentiating plateout from settling. Plateout should be more important in the case of Al_2O_3 and settling more important for UO_2.

2.3.3 X-ray diffraction identification of uranium oxides

Samples of collected uranium oxide aerosol from CRI-II have been analyzed both chemically and by x-ray diffraction for identification of the oxygen-to-uranium ratio and the crystal form of the oxide. Some of

ORNL PHOTO 2349-78

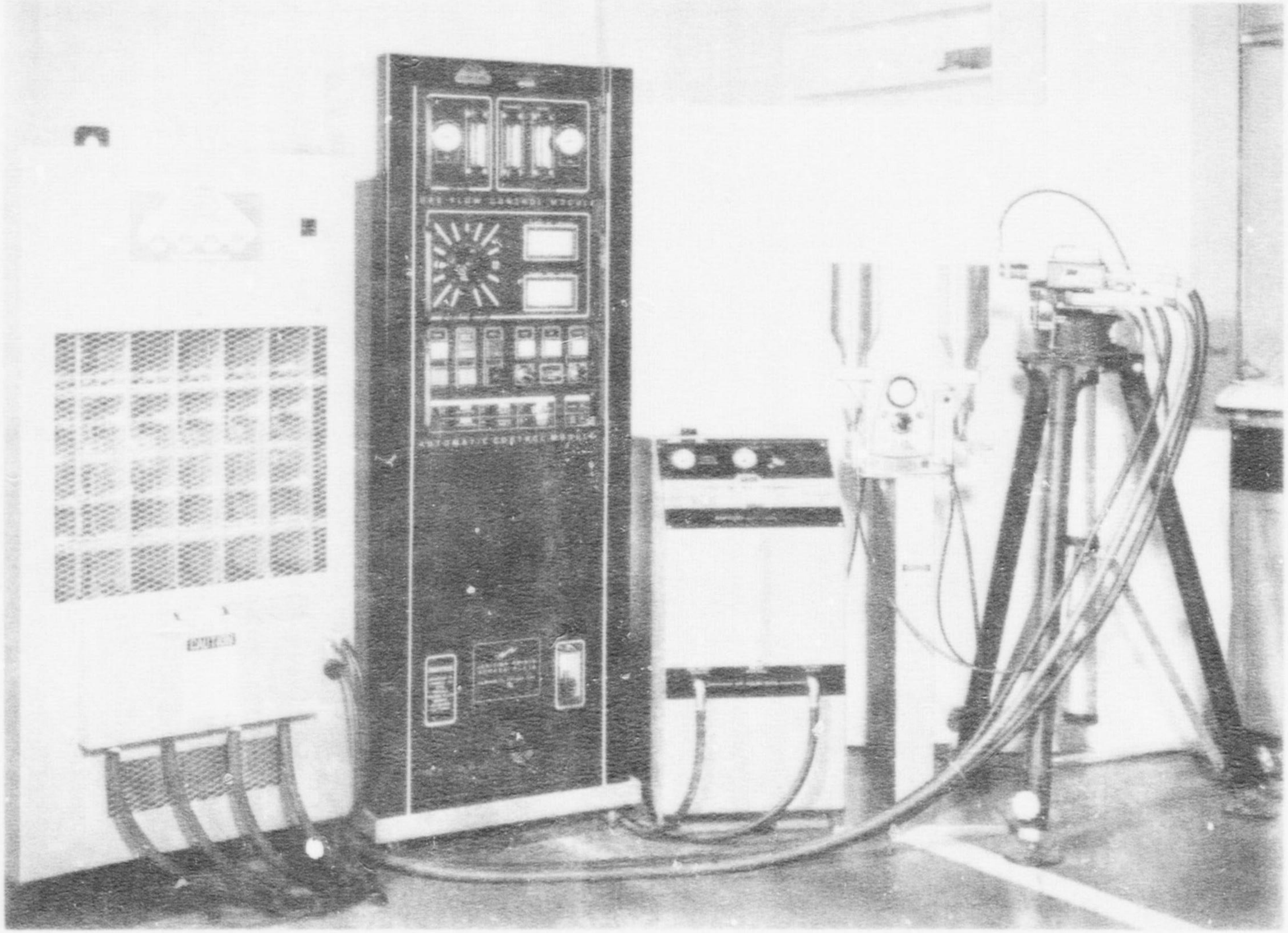

Fig. 9. Metco model 7M 80-kW plasma metal spray equipment for the NSPP.

Fig. 10. CRI-II metal-oxygen torch inside CRI-II vessel in operation.

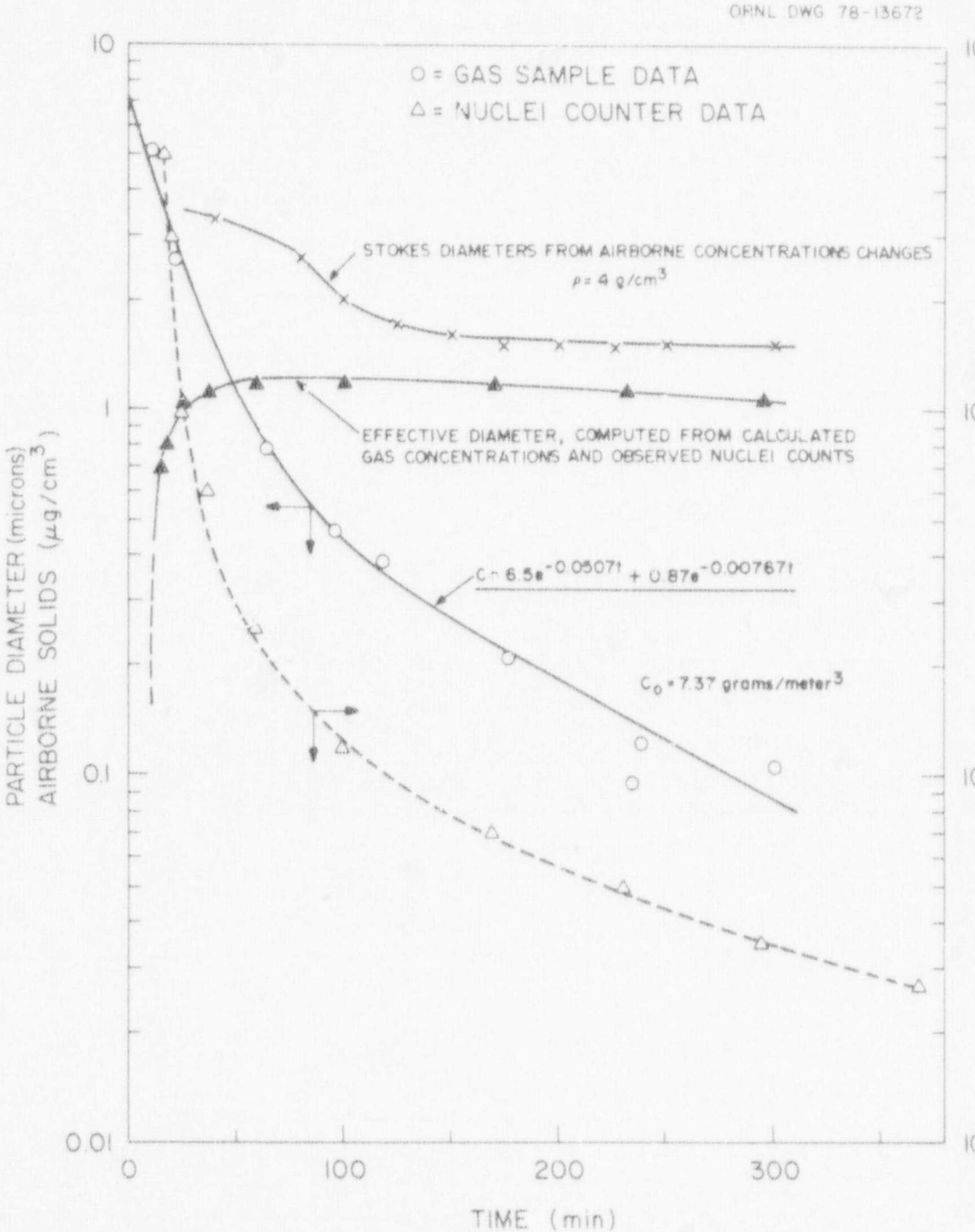

Fig. 11. Hisrograms of Al_2O_3 attenuation in CRI-II after 2-min aluminum burn.

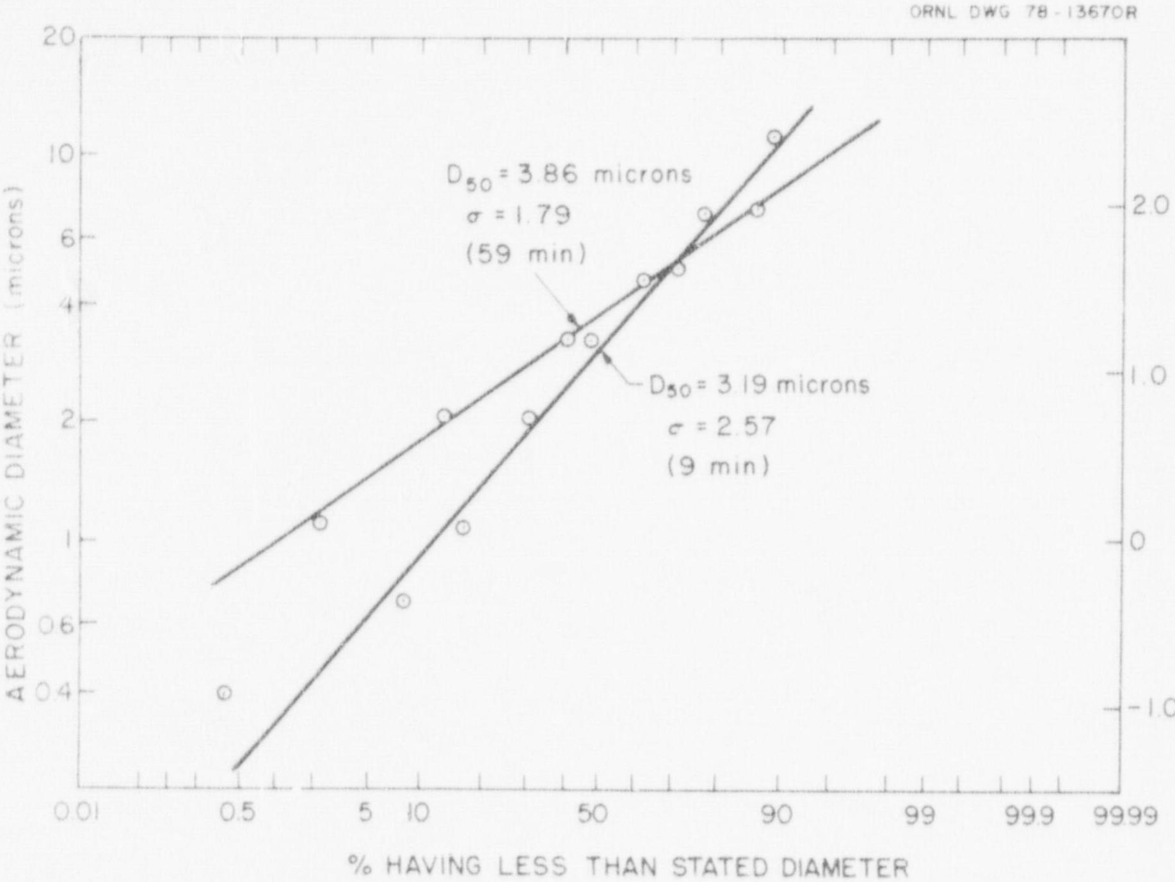

Fig. 12. Impactor analysis of Al_2O_3 agglomerates in CRI-II.

the samples have shown visual color differences, suggesting the presence of more than one form of oxide.

Wet chemical analysis of AF-8 and AF-9 gave an oxygen-to-uranium ratio of 2.2, which is the upper oxygen limit of the cubic crystal form of UO_2. For reference, the major diffraction lines of the simple uranium oxides were compared with AF-8, as shown in Fig. 14. No trace of oxide other than UO_2 is seen in the AF-8 pattern. Therefore, the excess oxygen indicated by the chemical analysis was present either as amorphous UO_3, which shows no diffraction, or as dissolved oxygen in UO_2.

This method, which is applicable to a sample of only a few milligrams of oxide, will be used routinely to confirm the form of oxide being produced by the metal-oxygen torch.

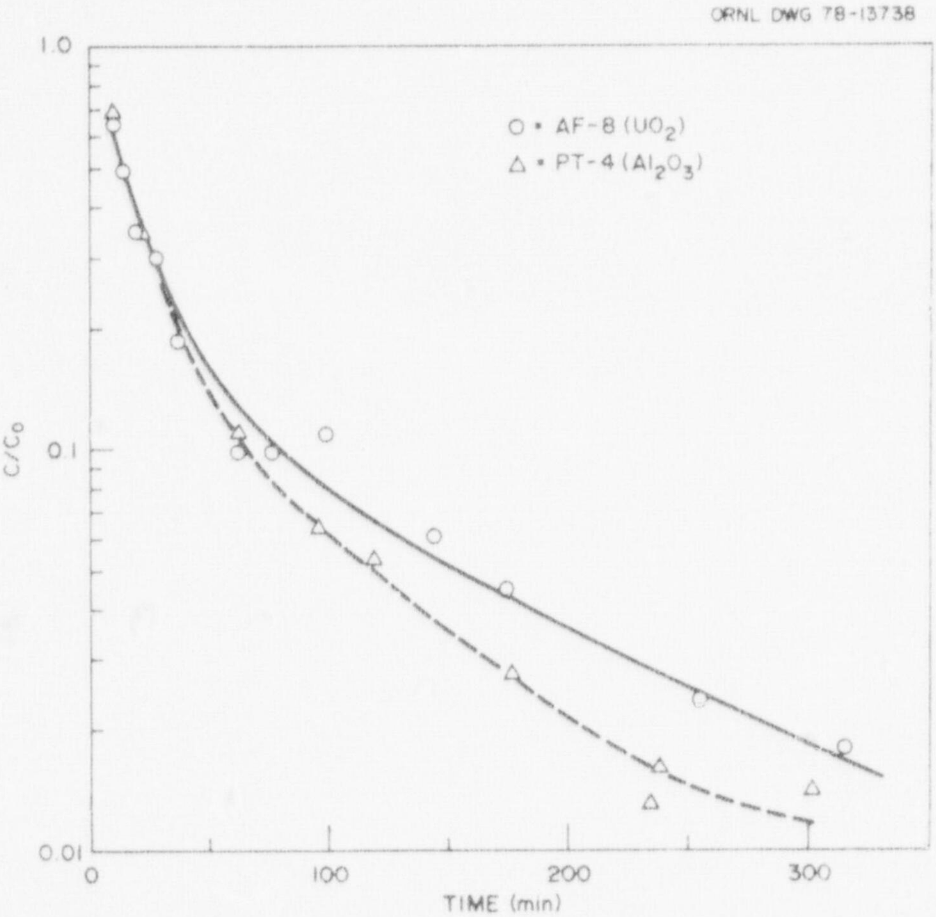

Fig. 13. Relative rates of change of aerosol concentration for Al_2O_3 and UO_2 in CRI-II.

2.3.4 Preparation of uranium metal powder for the plasma metal-oxygen burning experiments

Since the physical properties of the metal powder may either permit or inhibit ready transport through the metal powder feeders used in the torch, we have made some comparisons by sieve analysis and microphotography of the hydride-process uranium powder with the mechanically pulverized aluminum and tungsten that we now use as surrogates.

The uranium powder shown in Fig. 15 appears to have a size distribution closer to the aluminum, and both are considerably smaller than the tungsten. In the Avco feeder, we have obtained a maximum flow rate of about 35 g/min of aluminum and about 160 g/min of tungsten. No flow problems have developed with either.

ORNL-DWG 78-13668

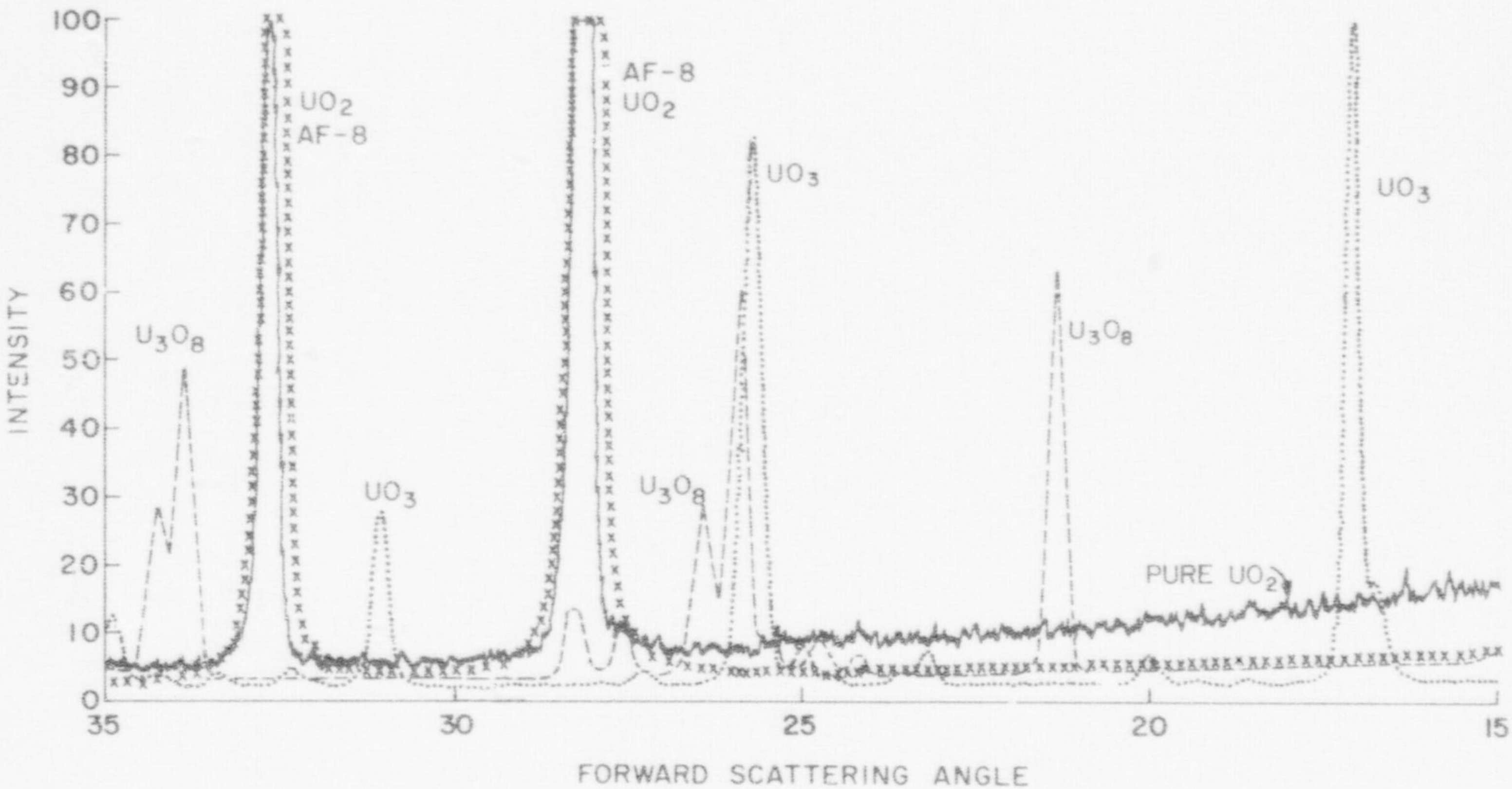

Fig. 14. Major x-ray diffraction spectra for various uranium oxides compared with arc-furnace UO_2 aerosol.

ORNL DWG 78-13810

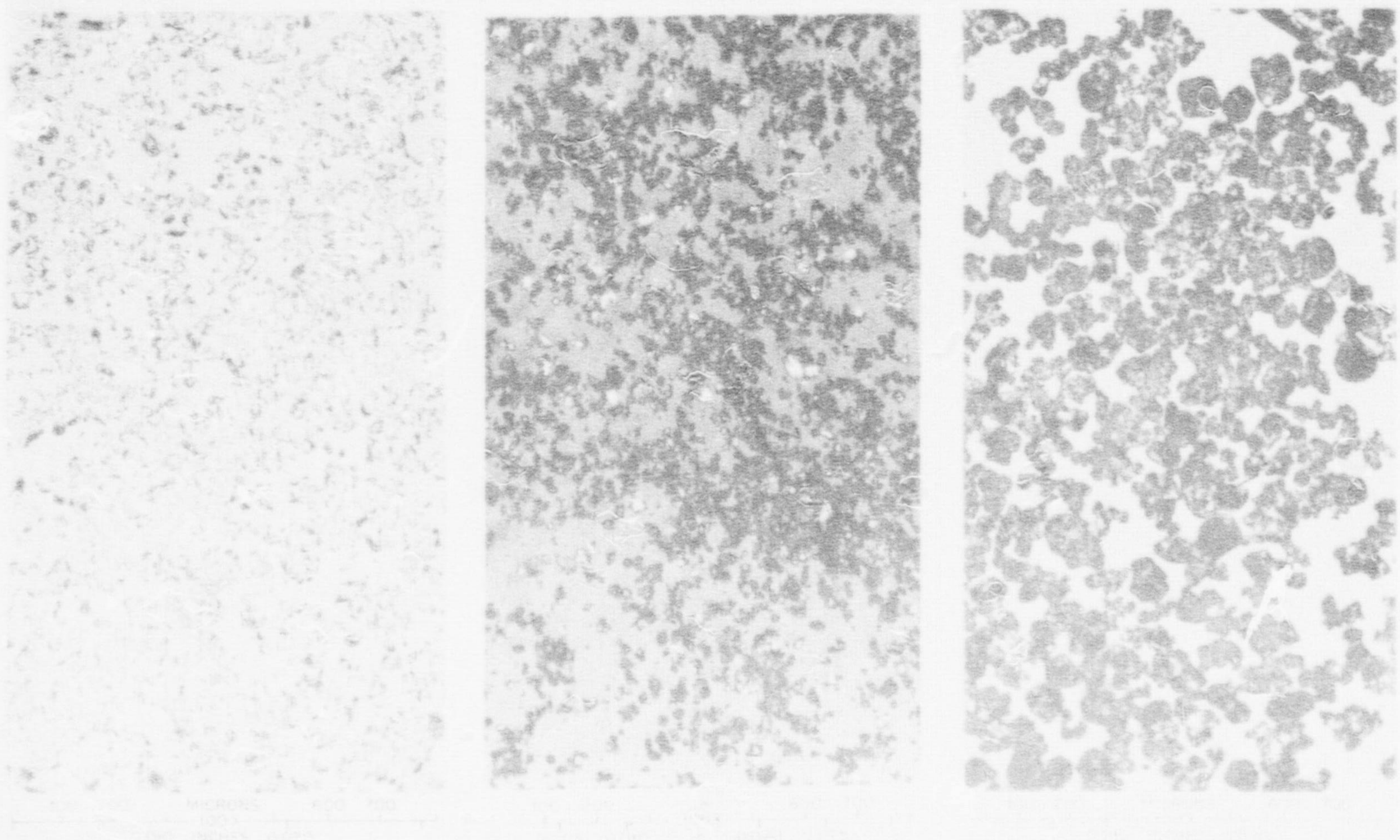

Fig. 15. Relative size distributions of commercial powdered metal aluminum and tungsten compared with uranium.

At our first opportunity to burn uranium, we will load only about 100 g into the hopper. We will hold the remainder in the dry box in the storage container in order to minimize the cleanup problem should the powder not feed properly. The fine particles could be removed by additional sieving if the present mixture does not feed satisfactorily.

3. ANALYTICAL PROGRAM

3.1 Source Term Evaluation

M. L. Tobias

3.1.1 Analysis of heat transfer, condensation and aerosol deposition in bubbles

Calculational method. A computer code based on the Continuous System Modeling Program (CSMP) system[2] was used to model some of the principal aspects of the bubble rise during a core-disruptive accident. The code exists in two forms, one to describe the rise of a sodium vapor bubble and the other for a UO_2 vapor bubble. In both cases, an inert gas (xenon) is assumed to be present. The main features of the code are described below.

1. The bubble size is controlled by heat transfer processes (principally condensation) and simple hydrostatic pressure effects. The more elaborate dynamics of the Rayleigh equation are not included.

2. Sodium side heat transfer is modeled by a plane interface heat conduction model which takes the simple form

$$\frac{dT}{dX} = 2.0 \frac{T_{L\infty} - T_i}{\sqrt{\pi \alpha_L t}} , \tag{1}$$

where

$T_{L\infty}$ = sodium temperature far from the interface,
T_i = sodium-vapor interface temperature,
α_L = sodium thermal diffusivity,
t = time.

3. The speed of the bubble rise follows the Davies-Taylor spherical cap model,[3] for which the bubble velocity is

$$v_\ell = 0.712\sqrt{gD} , \tag{2}$$

where D is the diameter of a sphere with the same volume as a spherical cap and g is the gravitational acceleration constant.

4. The condensation heat transfer model is based on the results of the Özisik-Kress approach.[4] The results of that study were incorporated into the code as a heat transfer coefficient varying hyperbolically with time:

$$h = \left(b + \frac{1 - b}{t + a}\, a\right) h_o \ . \tag{3}$$

For the present study, a = 1.0 and b = 0.1, representing rough approximations to the time dependence of the heat transfer coefficient. These assumptions are secondary in importance to the value taken for h_o.

5. Provision is made for computing heat losses from the bubble by radiation and other cooling mechanisms through heat transfer coefficients based on the temperature difference between the temperature of the main body of the bubble and either the saturation temperature of the condensing vapor or the bubble-sodium interface temperature:

$$q_j = h_j A \left(T_{bubble} - T_x\right) \ , \tag{4}$$

where q_j is the heat transferred by mechanism j of coefficient h_j, A is the bubble area, and T_x is the sink temperature. The interfacial area is that of a spherical cap: $A = 5.3155D^2$. As before, D is the diameter of a sphere with the same volume as the cap.

6. The bubble can be assumed to contain a steady heat source of arbitrary size to account for the energy of charged particle emissions (especially beta) from fission products and other reactor materials which might be carried up in the bubble. The energy from these particles would appear in the immediate vicinity of the bubble surface if no self absorption is assumed.

The calculation proceeds by determining the temperature at the interface from a heat balance of the bubble surface. This permits calculation of the condensation rate and of the bubble temperature, pressure, and volume as functions of time.

Calculational results. The results of calculations for bubbles composed of UO_2 vapor and inert gas rising in a pool of sodium are reported. (A few calculations were done for sodium—inert-gas bubbles for code checking purposes but because of their tentative nature they are not discussed.) Table 6 lists the range of the principal parameters varied in the study.

Table 6. Principal parameters covered in present study

Initial condensation heat transfer coefficient h_o, W/m^2-K	1, 10, 100, 1000
Initial bubble diameter,[a] m (ft)	0.3048, 3.048 (1, 10)
Bubble depth, m (ft)	1.1, 9.14 (~4, 30)
Initial vapor temperature, K	4000
Initial sodium-bubble interface temperature, K	838
Internal heat generation rate, MW/m^3	0, 0.6745[b]

[a]The diameter of a sphere of volume equal to that of the spherical cap.

[b]Corresponds to 10 MW in a 10-ft-diam sphere.

Figure 16 shows both the mass fraction of UO_2 vapor and the rise height in a 10-ft-diam bubble in a 30-ft pool of sodium for h_o = 100 W/m^2-K. The bubble takes about 2.5 sec to reach the surface; its position varies almost linearly with time. About 75% of the vapor condenses; the bubble contained about 13 kg of UO_2 at the start and 3.2 kg when it reached the surface. Figure 17 shows the bubble diameter variation for the same case. The decrease in hydrostatic pressure with rise compensates substantially for the quantity condensed, so that near the top, the bubble actually expands somewhat from its minimum value. Figure 18, however, demonstrates that the variation can be a strong function of the condensation rate, and if the condensation coefficients are sufficiently small, expansion is monotonic.

With the model used, interfacial temperatures did not approach the sodium boiling temperature. This was true of the sodium side conduction model represented by Eq. (1), which represents the temperature gradient

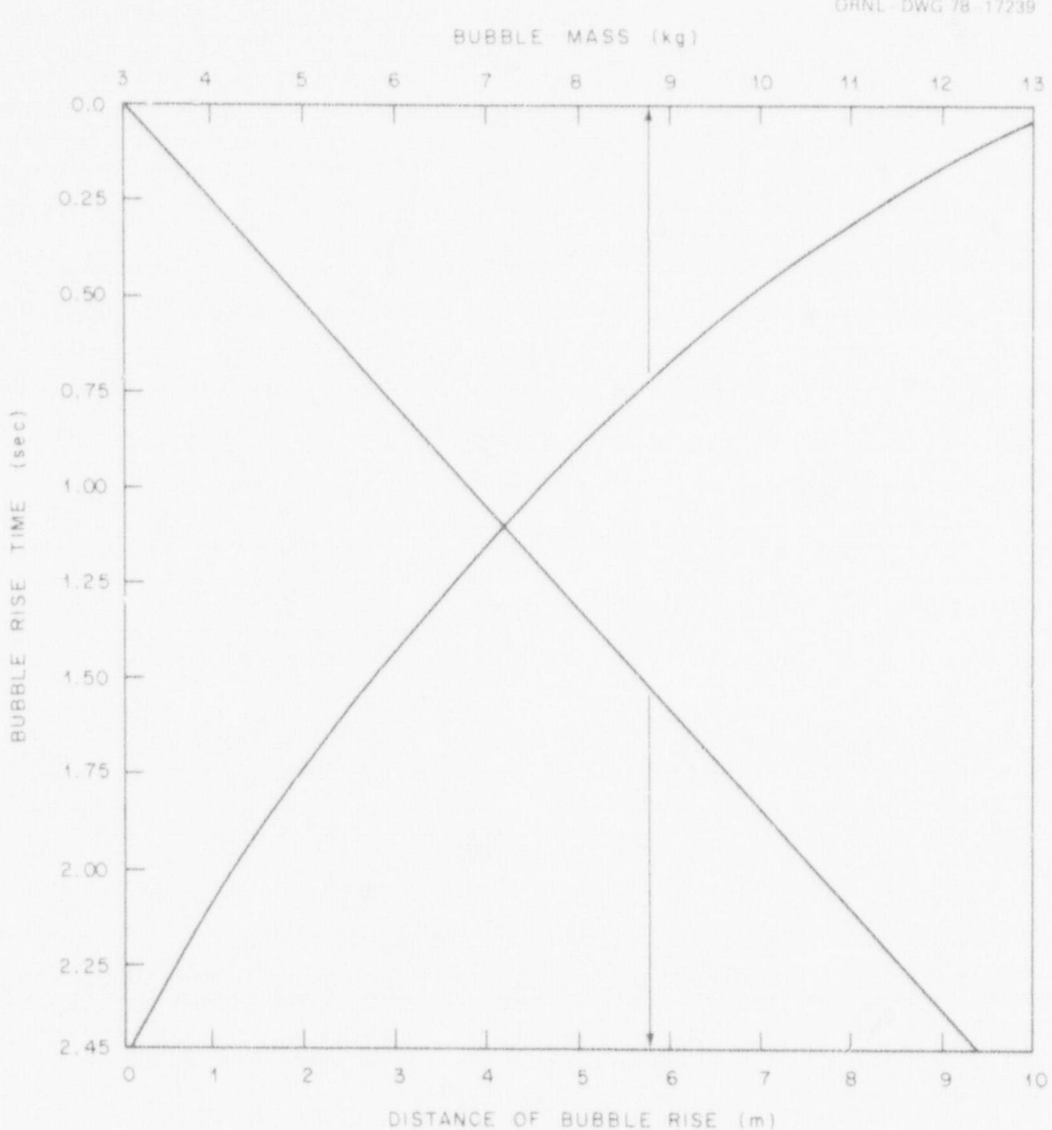

Fig. 16. Vapor mass in a nominal 3.05-m-diam (10-ft) bubble and height (rise) above the starting point vs time. Initial condensation coefficient 100 W/m^2-K, no internal radiation (beta) source.

for a linear rise in temperature at the interface. However, some calculations were done with half this gradient, corresponding to a constant interface temperature solution, and temperatures in excess of 1100 K were noted. This matter will be proved further. Figure 19 shows the interface temperature as a function of time for initial condensation coefficients of 1, 10, and 100 W/m^2-K. The rise in the interface temperature has little effect on the condensation rate since the driving force is

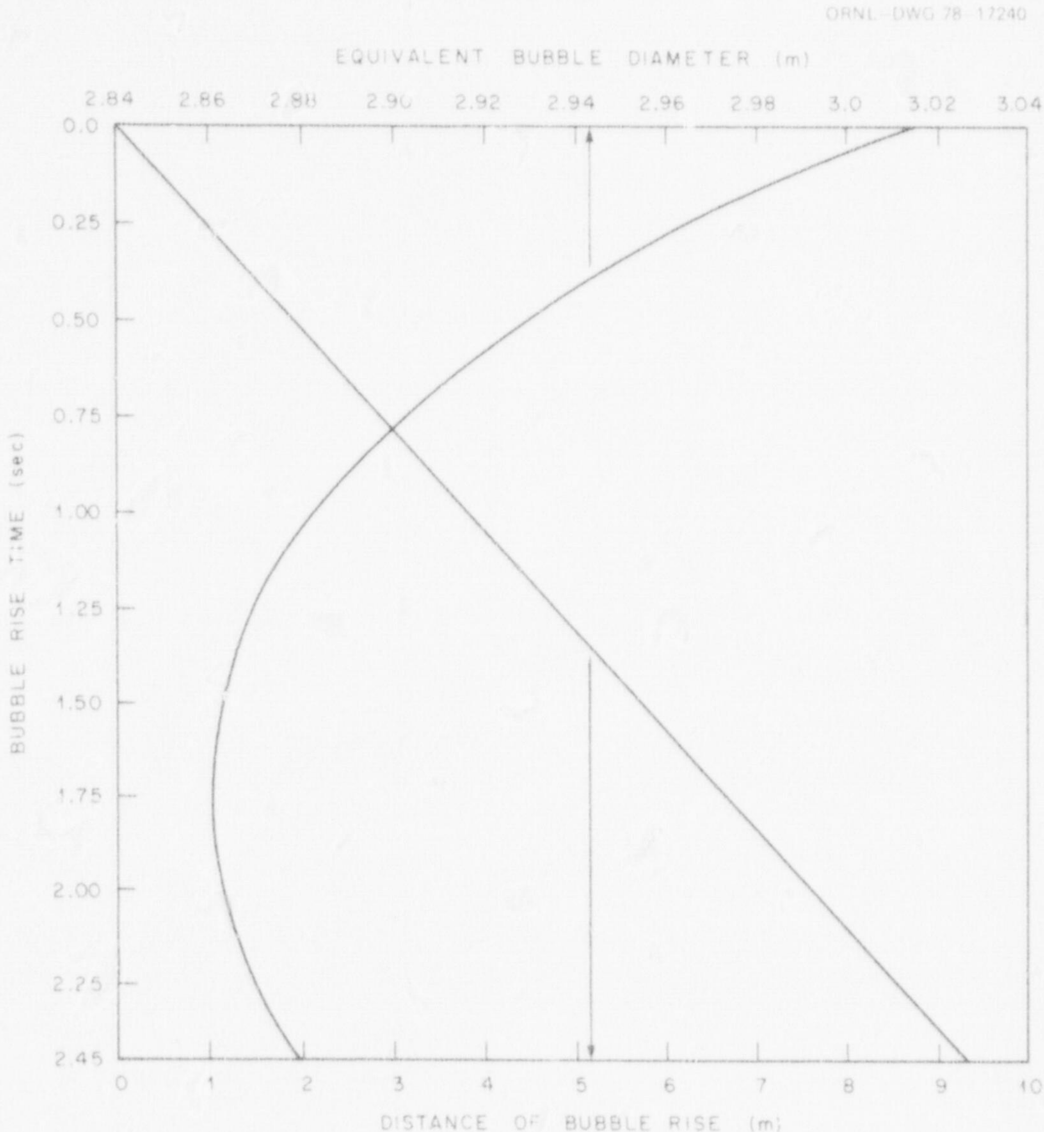

Fig. 17. Equivalent bubble diameter and rise vs time; same conditions as for case shown in Fig. 15.

the difference between the ∿4000 K vapor temperature and the interface temperature. The percent change in this difference is only mildly affected by the changes in interface temperature indicated here. This is more clearly brought out by Figs. 20 and 21, which show the effects of 10 MW of beta energy on interface and condensation rates. While Fig. 20 shows an ultimate difference in interface temperatures of 40 K, Fig. 21 shows that the condensation rate, indicated by the total amount condensed as a function of time, hardly changed.

ORNL DWG 78 17241

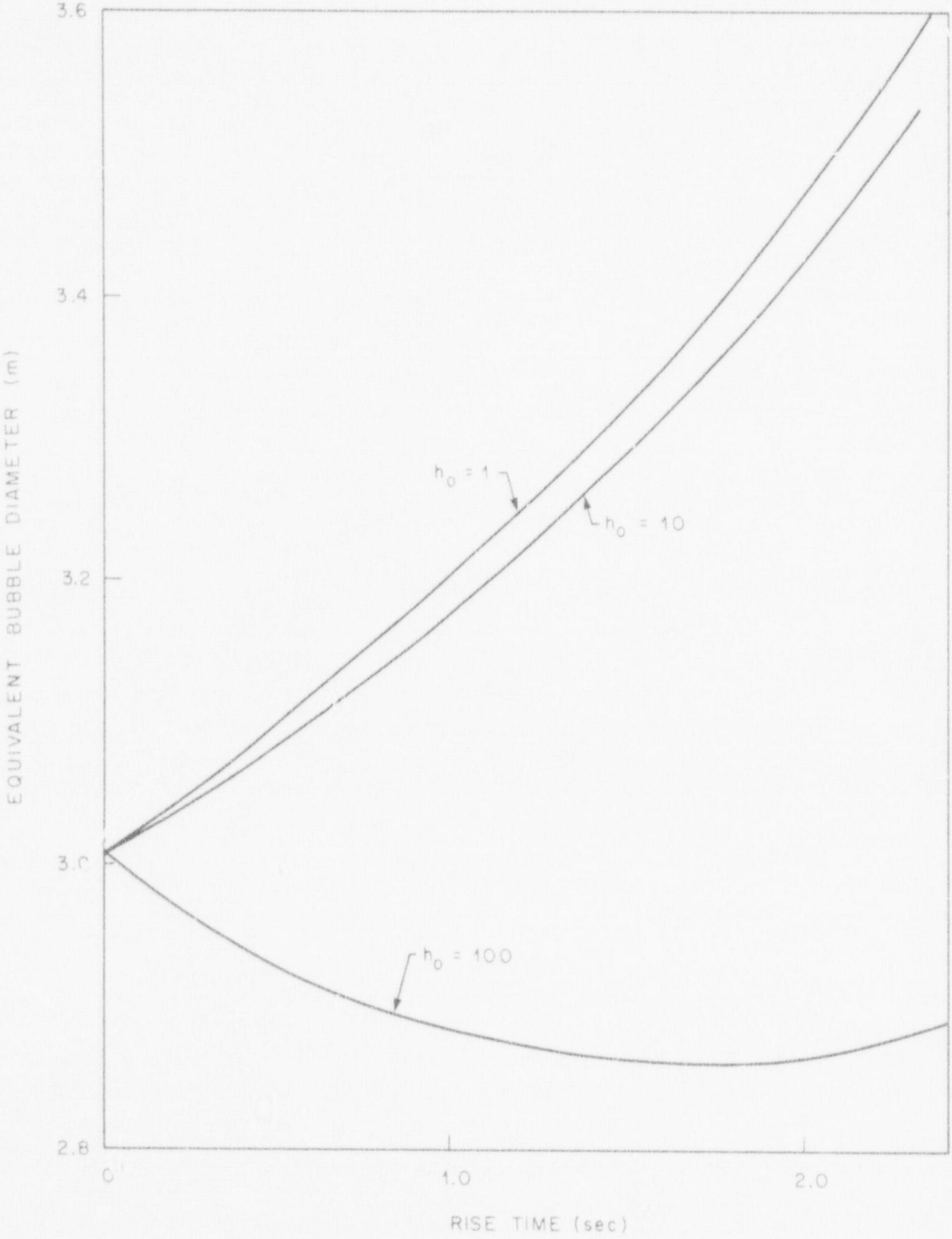

Fig. 18. Equivalent bubble diameter vs time for initial 3.05-m-diam (10-ft) bubbles and various initial condensation coefficients (W/m^2-K).

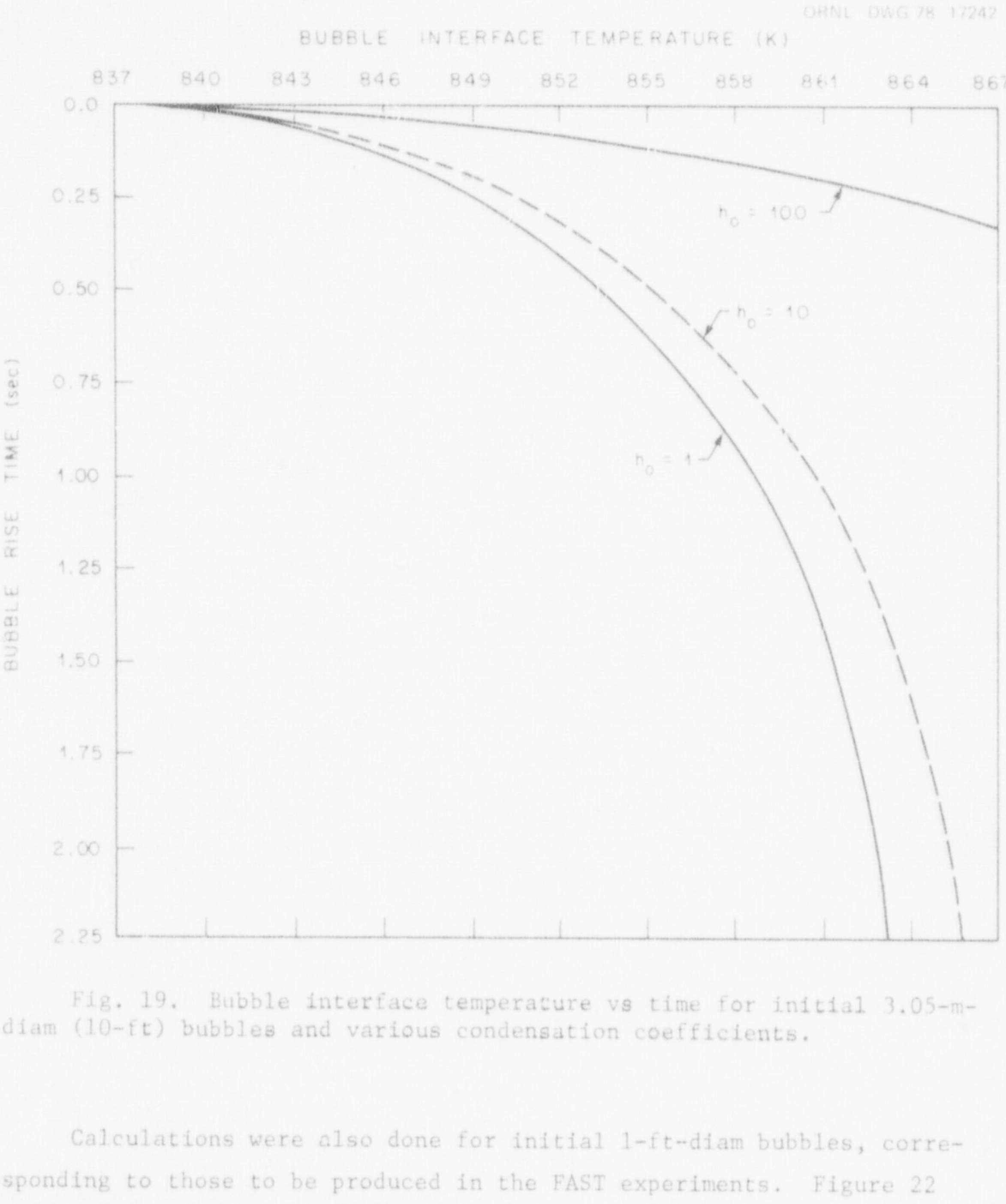

Fig. 19. Bubble interface temperature vs time for initial 3.05-m-diam (10-ft) bubbles and various condensation coefficients.

Calculations were also done for initial 1-ft-diam bubbles, corresponding to those to be produced in the FAST experiments. Figure 22 illustrates the most striking result, namely, that except for the lowest condensation coefficients, vapor condensation was complete within a very short distance of rise (~0.1 m). The effect of an internal heat source was found to be even less than that for the 10-ft bubble.

Using the data obtained for a 10-ft bubble, a HAARM-2 calculation was performed assuming that all the vapor condensed converted to an

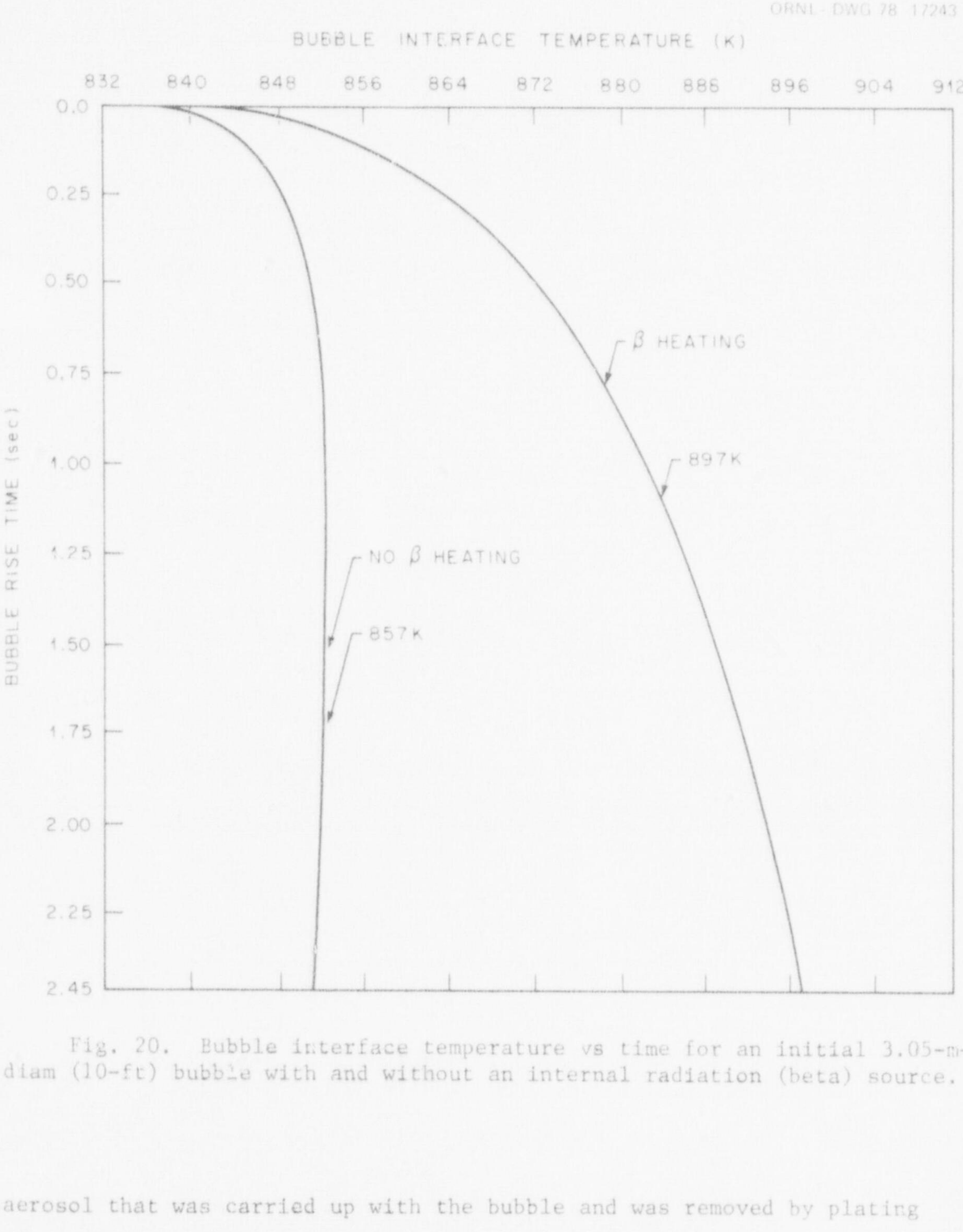

Fig. 20. Bubble interface temperature vs time for an initial 3.05-m-diam (10-ft) bubble with and without an internal radiation (beta) source.

aerosol that was carried up with the bubble and was removed by plating or settling. The bubble was treated as a 10-ft chamber. About 85% of the hypothetical aerosol remained suspended; the remainder plated out thermophoretically, with only a small quantity settling. Initial aerosol parameters were R_{50} = 0.0225 μm and σ = 1.9, taken from previously

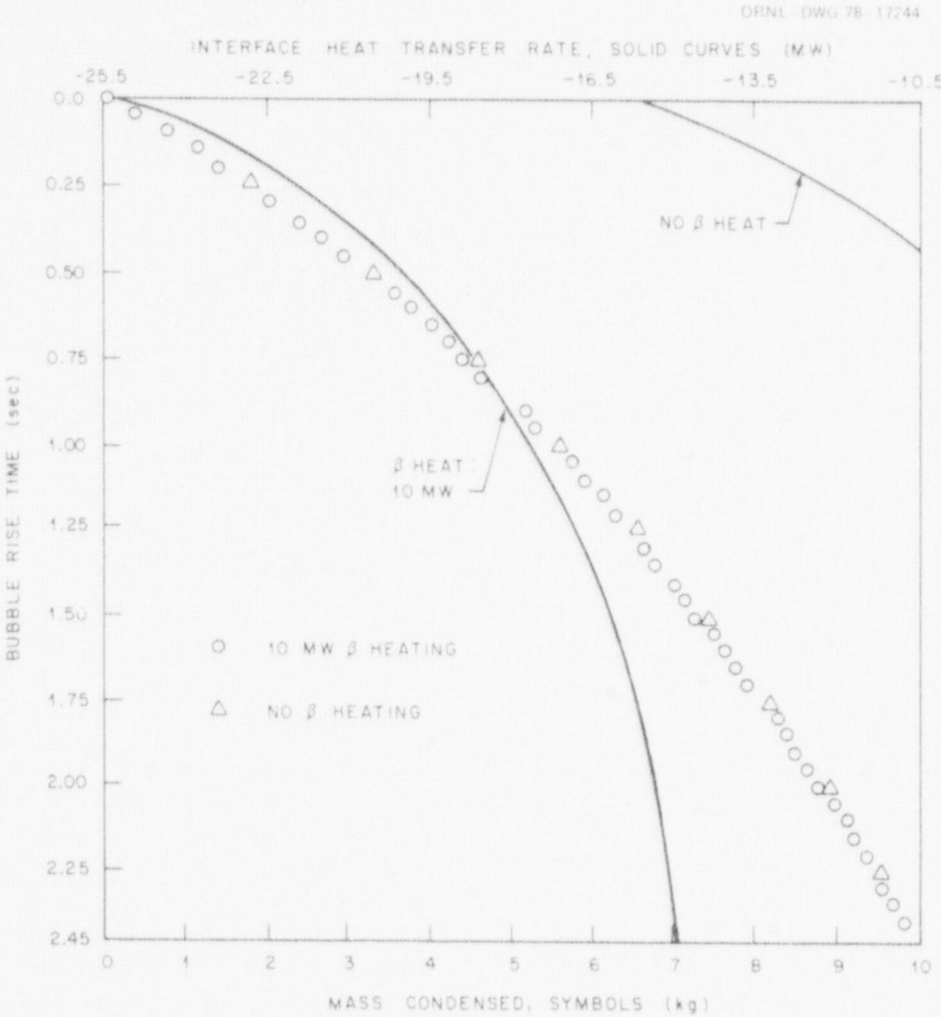

Fig. 21. Amount of vapor condensed (kg UO_2) and heat transfer rates with and without beta heating.

reported CRI-III measurements. The suspended particles grew to about 0.147 μm with σ = 1.969.

The results of this study indicated some areas where model improvement is needed. First, the heat transfer coefficient for condensation used should be more closely coupled to that determined by separate analyses (i.e., that of Özisik and Kress). Second, the modeling of bubble cooling needs improvement to include a better approach to radiation heat loss and the possibility of the vapor reaching saturation temperatures. Third, the sodium side heat transfer calculation should perhaps be more elaborate, but this may not be necessary if heat loss rates continue to prove insensitive to the interface temperature.

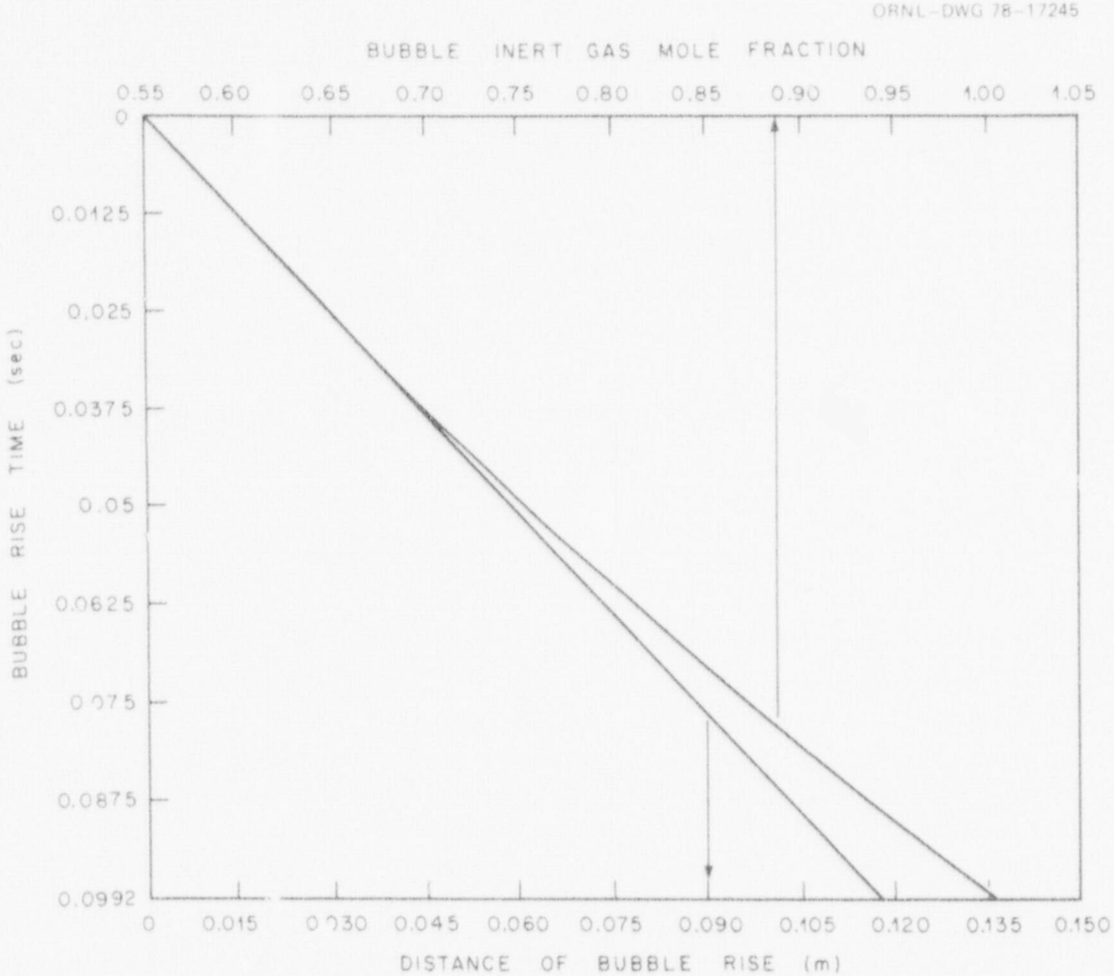

Fig. 22. Bubble inert gas mole fraction and bubble height vs time for a nominal 0.30-m-diam (1-ft) UO_2 vapor bubble. Total vapor condensation was calculated at ~0.12 m. Total pool depth was 1.1 m.

3.1.2 Comparison of AEROSIM and HAARM-2 and -3 codes

The AEROSIM program, a British code developed to model aerosol transients, and the associated differential equation solving program FACSIMILE have been made operational on the IBM 360/195 computer at the Oak Ridge Gaseous Diffusion Plant. Test cases have been successfully run, and some comparisons with HAARM-2 and HAARM-3 calculations have been made. Both codes were used to make pretest predictions for NSPP run 301, the first run where both uranium oxide and sodium oxide aerosols were to be present.

REFERENCES

1. T. S. Kress, *Breeder Reactor Aerosol Release and Transport Program Quart. Proj. Rep. January–March 1978*, ORNL/NUREG/TM-213.

2. *Continuous System Modeling Program III (CSMP III) Program Reference Manual*, IBM Corporation Manual SH 19-7001-3, Fourth Edition (December 1975).

3. R. M. Davies and G. I. Taylor, *Proc. Royal Soc. London, Ser. A* 200A, 375 (1950).

4. M. N. Özisik and T. S. Kress, "Effects of Internal Circulation Velocity and Noncondensible Gas on Vapor Condensation from a Rising Bubble," *Nucl. Sci. Eng.* 66, 397–405 (1978).

NUREG/CR-0340
ORNL/NUREG/TM-244
Dist. Category R7

Internal Distribution

1. R. E. Adams
2. M. Bender
3. H. W. Bertini
4. J. R. Buchanan
5. W. B. Cottrell
6. G. F. Flanagan
7-9. M. H. Fontana
10. J. T. Han
11. H. W. Hoffman
12-19. T. S. Kress
20. Milton Levenson
21. R. E. MacPherson
22. F. R. Mynatt
23. G. W. Parker
24. L. F. Parsly
25. P. Patriarca
26. J. M. Rochelle
27. Myrtleen Sheldon
28. A. M. Smith
29. I. Spiewak
30. A. L. Sutton, Jr.
31. D. G. Thomas
32. M. L. Tobias
33. H. E. Trammell
34. D. B. Trauger
35. J. L. Wantland
36-37. J. S. White
38. G. D. Whitman
39-41. A. L. Wright
42-43. Central Research Library
44. Y-12 Document Reference Section
45-47. Laboratory Records Department
48. Laboratory Records (RC)

External Distribution

49. J. T. Larkins, Experimental Fast Reactor Safety Research Branch, RSR, Nuclear Regulatory Commission, Washington, D.C. 20555
50. Director, Research and Technical Support Division, DOE-ORO
51-340. Given distribution as shown in category R7 (25 copies — NTIS)

U.S. GOVERNMENT PRINTING OFFICE 1977-748-189/264